SYNTHESIS AND CHARACTERIZATION OF SILVER NANO PARTICLES DOPED REDUCED GRAPHENE OXIDE FOR METHANE GAS SENSING AT ROOM TEMPERATURE

By

Ayesha Tasawar

Kholah Mehtab

Muhammad Ali Raza

School of Chemical & Materials Engineering

National University of Sciences & Technology

2020

SYNTHESIS AND CHARACTERIZATION OF SILVER NANO PARTICLES DOPED REDUCED GRAPHENE OXIDE FOR METHANE GAS SENSING AT ROOM TEMPERATURE

By

Leader - Reg # 177813 Ayesha Tasawar

Member 1- Reg # 173981 Kholah Mehtab

Member 2 - Reg# 177013 Muhammad Ali Raza

School Of Chemical & Materials Engineering (SCME)

National University of Sciences & Technology (NUST)

July, 2020

Submitted to
National University of Sciences and Technology
In partial fulfillment of the requirements
For the degree of

BACHELOR IN MATERIALS & METALLURGICAL ENGINEERING

2020

ABSTRACT

This paper is devoted to an investigation on the methane sensing properties of graphene (G), decorated with silver nanoparticles (AgNPs), at room temperature. Graphene has noteworthy logical consideration in light of its extraordinary compound, mechanical and electrical properties. This exceptionally solid two dimensional (2D) material has forthcoming application in gas sensors. Methane gas sensor are significant for human wellbeing and security. Methane is profoundly lethal gas and intense to identify in view of its drab, and can get into human blood through lungs or skin. It moves into the tissues where it ties with oxygen and lessening the measure of oxygen there. This prompts cerebral pain, wooziness, disarray and even demise at high focus and long-lasting introduction. Thus, we report the utilization of Graphene, surrendered Graphene (as a rule called diminished Graphene Oxide), and silver nanoparticles/Graphene Nano composite film for methane detecting at surrounding conditions. The AgNP/rGO film on substrate is then used, as a resistivity-based sensor, to examine its response to the presence of methane gas. Our results show sensing of methane concentrations up to 150 sccm, the maximal response increases linearly and rapidly, even at room temperature. Moreover, we demonstrate that AgNPs/rGO is of low limit of detection, highly stable, selective, and reversible for methane sensing. Our prototype thus promise a low-cost and simple-to-fabricate methane sensing device

Keywords: Graphene Oxide, Reduced Graphene Oxide, Silver nanoparticles, Methane

CERTIFICATE

This is to certify that work in this thesis has been completed by Ms. Ayesha Tasawar, Ms. Kholah Mehtab, and Mr. Muhammad Ali Raza under the supervision of Dr. Adeel Umer and Dr. Farooq Zafar at the School of Chemical and Materials Engineering, National University of Sciences and Technology, H-12, Islamabad, Pakistan.

Supervisor:

Dr. Adeel Umer
Department of Materials Engineering
School of Chemical & Materials Engineering,
National University of Sciences and Technology.

Co- Supervisor:

Dr. Farooq Zafar
NESCOM
Islamabad.

Submitted through:

HoD: Dr. Zakir Hussain
Department of Materials Engineering
School of Chemical and Materials Engineering
National University of Sciences and Technology.

Dean: Dr. Arshad Hussain
School of Chemical and Materials Engineering
National University of Sciences and Technology.

Dedication

This work is dedicated to all those who carve a path for themselves despite sheer hardships and opposition. This work is symbol of courage and commitment for those who feel exhausted and loose hope. This work is dedicated to loving parents and honest friends who believe in you.

Acknowledgment

Praise be to Allah, the Cherisher and Sustainer of the worlds; (Surah Al-Fatiha, 1)

Our special recognition and gratitude for our supervisor Dr. Adeel Umer, whose support and guidance kept us motivated throughout the project.

We would also like to extend our regards to our co-supervisor, Dr. Farooq Zafar and Sir Ejaz Toba whose precious suggestions regarding the experimentation and the constructive criticism has polished our work and has made it appreciable.

We would like to pay gratitude to the supporting staff of SCME with special mention of Mr. Ahsan Wajid who mentored and supported us consistently and Mr. Muzammil for their assistance during the experimentation and research.

Last, but not the least, this achievement would not have been possible without the support and prayers of our parents and friends. They are the ultimate source of inspiration and courage for us who stood by us through thick and thin.

TABLE OF CONTENTS

LIST OF TABLES

LIST OF FIGURES

ACRONYMS LIST

GO *Graphene Oxide*

rGO *Reduced Graphene Oxide*

N-doped rGO *Nitrogen doped Reduced Graphene Oxide*

AgNP *Silver Nano Particles*

SEM *Scanning Electron Microscope*

XRD *X-ray diffraction*

FTIR *Fourier Transform Infrared*

2D *2 Dimensional*

3D *3 Dimensional*

RT *Room temperature*

CHAPTER 1

INTRODUCTION

1.1 Abstract:

Gas sensors are gadgets that convert a gas volume division into electrical signs, and they are generally utilized in numerous fields, for example, ecological checking. Graphene is another sort of two-dimensional precious stone material that has numerous brilliant properties including huge explicit surface territory, high conductivity, and high Young's modulus. These highlights make it in a perfect world appropriate for application for gas sensors. Right now, primary attributes of gas sensor are first presented, trailed by the readiness strategies and properties of graphene. Likewise, the advancement procedure and the condition of graphene gas sensors are presented insistently as far as structure and execution of the sensor. The development of new competitors including graphene, polymer and metal/metal oxide composite improves the exhibition of gas recognition altogether. At long last, the away from of graphene gas sensors for what's to come is given by the most recent research results and patterns. It gives guidance and thoughts for future research.

1.2 Introduction

Design of efficient methane gas (CH_4) sensing devices with large industrial applications has been a challenging task for several decades. Interest in this task has grown with developments in the petrochemical industry, which is still an active research field. However recent studies point to the fact that methane gas has reached an unacceptable level in the world. Along these lines, in medical diagnosis we may also mention recent uses of CH_4, specific doses. To this end, it is most desirable to design practical low-cost methane gas sensors which operate readily at low temperatures. The sensor must also be of high sensitivity and thumbnail sizes. Because the CH_4 sensors currently suffer from low

sensitivity, high power consumption, high cost, etc. research on novel materials for compensating such shortcomings is of much interest. It should be noted that the current low-cost metal-oxide-based CH4 sensors commonly operate at relatively high temperatures and thus consume considerable power. As in the present graphene manufacturing state, a single sheet of carbon honeycomb structure has made this material commercially available, we take advantage of the graphene properties when decorated with silver nanoparticles, to propose a novel methane gas sensor. Together with the graphene properties, the findings of the present work pave the way for the creation of a Nano scale methane gas sensor, which satisfies a reasonable portion of the desired demands. When designing a sensing device, a comparison is normally made for any object between the changes in the physical properties of the main elements that shape the device, in the presence and absence of the entity. Such changes could include temperature variations, mechanical properties, and electrical and/or optical properties. Due to the accuracy and ease of measurements, conductance (resistance) of the sensing material is of considerable importance among those physical properties. To this end, the resistance (conductance) of the material chosen should vary considerably and rapidly.

1.3 Introduction to Methane

Methane is a gas that is colorless. It is odorless at low concentrations, but at high concentrations it has a sweet smell. At mixtures more than about 5-15% in air, it is explosive. It has a lifetime of around ten years because it is only very gradually destroyed by other chemicals in the air. Methane is one of a group of chemicals known as volatile organic compounds (VOCs). It is produced both naturally and from man's activities.

Methane is the major component of natural gas used for domestic and industrial heating and for generating electricity at power plants. It's also used to produce many more complex chemical compounds in the chemical industry.

1.4 Common Sources of Methane and Safety Limits

One of the main sources of methane into the environment is from the natural decomposition

of plant and animal matter in airless conditions. This occurs in marshes, rice paddies and the guts of animals.

Methane (CH_4), ***is an odorless gas that is flammable or explosive at concentrations of 5% to 15% by volume of air*** [NIOSH 1985b].

On a local scale, methane build-up poses an explosion hazard that can result in area evacuation over old landfills or mines. Methane does not contribute significantly to the formation of ground level ozone or photochemical smog as compared with other volatile organic compounds (VOCs). The main impact of methane is on a global scale, as a greenhouse gas. Although levels of methane in the environment are relatively low, its high "global warming potential" (21 times that of carbon dioxide) ranks it amongst the worst of the greenhouse gases.

At normal environmental concentrations, methane has no impact on human health. At extremely high (artificial) concentrations in an enclosed space the reduction in oxygen levels could lead to headache, dizziness, confusion and even death at high concentration.

1.5 Emissions of Methane

The primary hazard presented by methane is its flammability when sufficient quantities accumulate in a mixture with atmospheric oxygen. When methane concentrations are below 50,000 ppm the gas mixture is too 'lean' and there is insufficient methane for combustion. Above 150,000 ppm, the gas mixture is too 'rich' and insufficient oxygen exists for combustion. When methane is present at concentrations between 50,000 and 150,000 ppm it has the ability to combust.

Category 1: 1,000 to 9,999ppm (less than 1% of air)

Category 2: 10,000 to 49,999ppm (1% to less than 5%)

Category 3: 50,000ppm or greater (5% or greater of air)

It is important to remember that methane does not exist the same way CO2 does in the atmosphere. Methane undergoes chemical reactions in the atmosphere, and within ten years it degrades to CO2 and water. The inclusion of this resultant CO2 when assessing methane's

overall impact is referred to as feedback and the degradation of methane in the atmosphere is known as a methane sink. If the amount of methane being absorbed through the sink effect exceeds the amount of methane emissions in each period, total levels of methane will fall. The global methane emissions and sinks, often referred to as a methane budget, are summarized in Figure. There are three main types of methane emissions: Biogenic – wetlands, rice paddies, cows, landfills, etc. Thermo genic – deriving from either natural seeps from fossil fuel or as a result of exploration and production (E&P) and coal mining activities Pyrogenic – the result of incomplete combustion of biomass (for example, forest fires), biofuels, and fossil fuels.

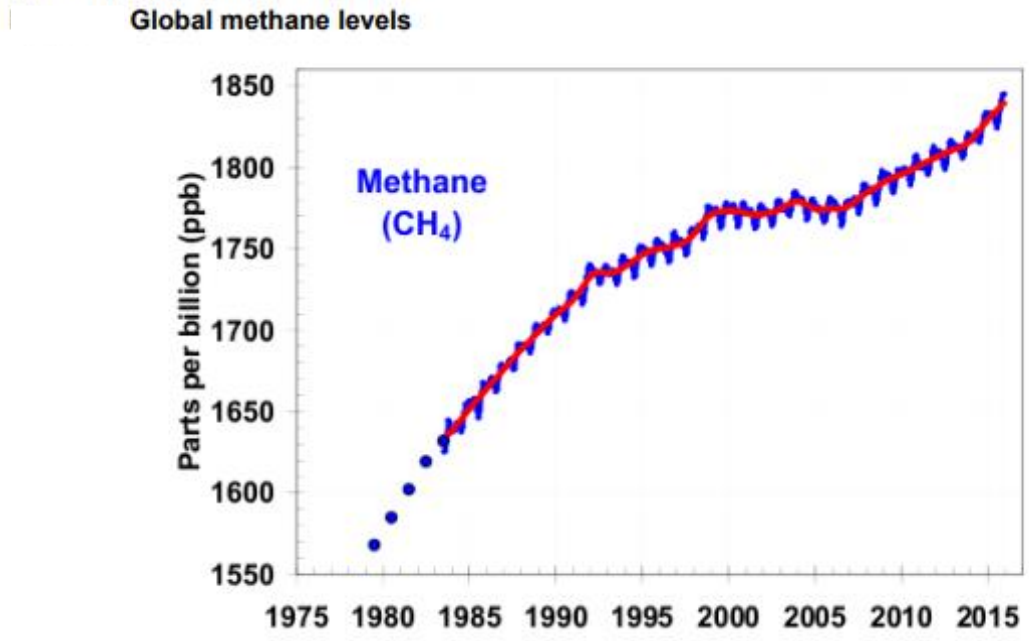

Figure 1: the drastic increase in methane levels

Within these categories, a distinction can be made between natural and anthropogenic sources. So, emissions of anthropogenic methane from fossil fuels will be partly thermo genic and partly pyrogenic. The Global Carbon Project estimates that production and use from the fossil fuel sectors generate between 77 and 133 million tons of methane per year. This figure shows the overall 2003-2012 carbon budget showing both natural and anthropogenic sources and the effect of the methane trap that reduces, but does not eradicate, global methane emission production.

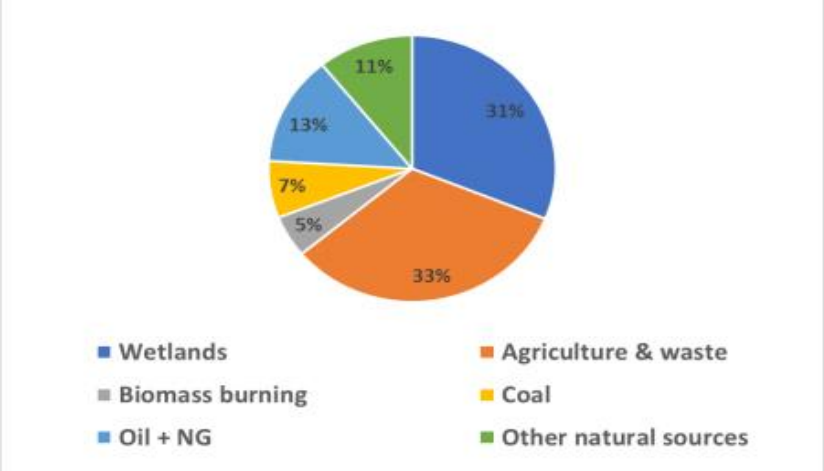

Figure 2: methane consumption

1.6 Few historic events of CH4 poisoning

A gas well blowout in Belmont County, Ohio was leaking methane, a potent greenhouse gas, into the atmosphere in February and March 2018. Satellite data analysis has now shown that the relatively unknown leak was one of the country's most important leaks ever to occur. A research group found that gas leaked approximately 120 metric tons of methane per hour over a 20-day period. This amounted to a total of more than 50,000 tons of methane.

Another incident in which a natural gas spill in the mountains above Los Angeles was one of the worst unintended greenhouse gas discharges in US history. A recent analysis reveals that the months-long tragedy contributed to the release of 97,100 metric tons of methane into the atmosphere. The methane emissions from the leak, caused by a ruptured pipe, effectively doubled the methane emissions of the entire Los Angeles metropolitan area, creating enough pollution to match the annual output of nearly 600,000 cars.

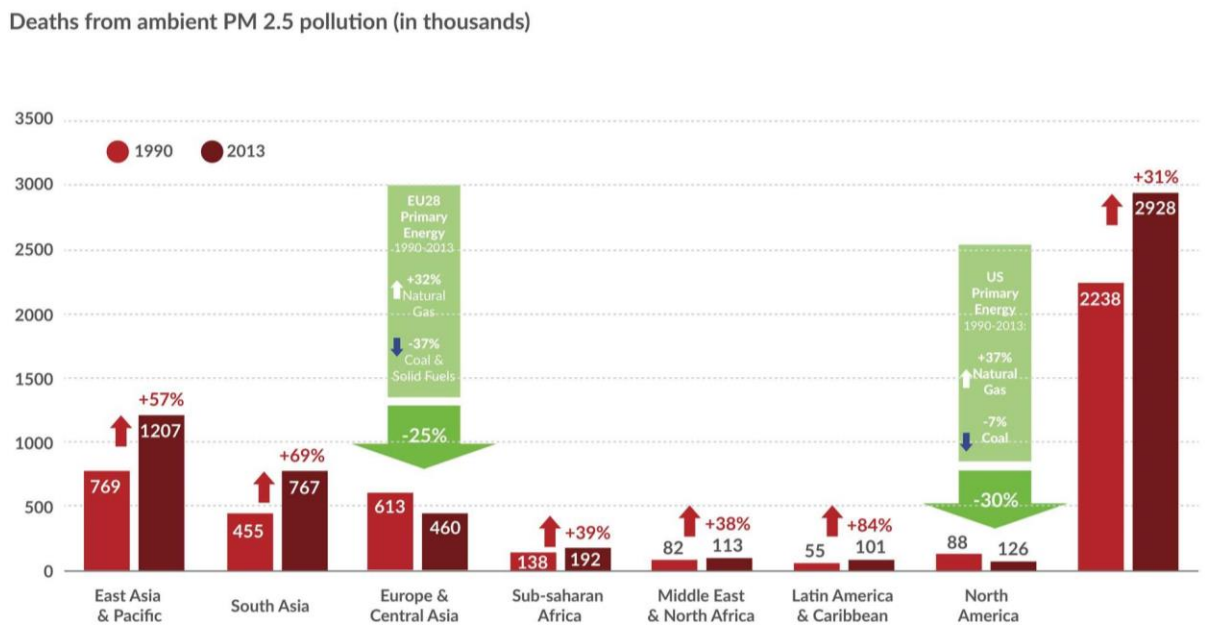

Figure 3: Deaths caused by methane

1.7 Solid State Methane detectors

The working principle of this type of gas sensors is the revocable contact of gas molecules with sensing material, this interaction alter the electric resistance of sensor, this change in resistance measured as signal. Solid-state gas sensors can be electrochemical or chemi-resistive.

An electrochemical sensor is very similar to a fuel cell. Electrochemical sensors comprise of electrodes dipped in the electrolyte (usually sulfuric acid) and connecting wires. The REDOX reaction of carbon monoxide occur on electrodes which produce current and this current is measured as a signal.

Chemi-resistive sensors consist of a thin sensing material which is connected to an integrated circuit. Oxygen chemisorbed on sensing element and increase the resistance of the sensor, as the sensor exposed to target gas change in resistance occurs which measured as the response. Because of simplicity and low cost, focus will be on chemi-resistive sensor. However, the sensing mechanism of chemi-resistive gas sensor is multifaceted and under

research.

1.8 Materials for Solid State Sensors

The use of material for solid-state gas sensors is without limitations. A sensor should be generally high in sensitivity, selectivity and stability. Electronic structure, adsorption / desorption characteristics, catalytic activity, band gap, electrical conductivity and thermodynamic stability greatly influence the choice of sensing material. Graphene meets a number of requirements, primarily sensitivity, selectivity and stability required in sensing materials. According to Schedin et al. graphene's study, it can provide ultimate protection, as graphene has low electrical noise compared to conventional semiconductors and fast transfer of catalytic electrons.

1.9 Introduction to Graphene

Graphene has 2D structure that consists of carbon atoms hybridized by Sp2 and arranged in a hexagonal pattern. The form of arrangement is called structure of the honeycomb. Graphene possesses remarkable mechanical, electrical and very high unique surface properties. Thanks to the covalent nature of the bonding and the limited bond length, high mechanical strength. High electrical conductivity and low electrical noise is because of no band gap between valence and conduction band. The electron mobility in graphene is about 100 times greater than any other conductive material, and it has the ability to tolerate high concentrations of electrical current. Graphene is totally impermeable to all gasses and has a high capacity for adsorption. Such two properties are of great value in applications for gas sensing. As graphene is considered “the next wonderful material” however to replace currently used materials in electronics with graphene is still debating. Carbon atoms in graphene are Sp2 hybridized, Sp2 hybridization yield three Sp2 orbitals that are arranged at 120 degrees and one un-hybridized orbital which form delocalized electron cloud just like benzene.

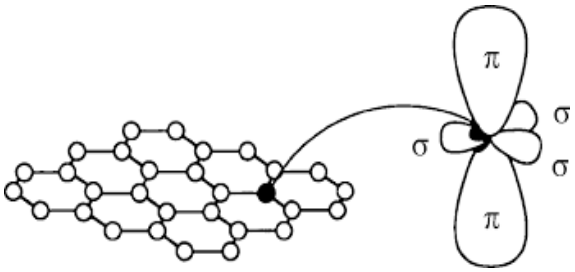

Figure 4: hybridization of graphene

1.10 Routes for Graphene Preparation

In 1859, by chemical method Benjamin Brodie provided the basis for graphene synthesis, he studied graphite reaction with oxidizing agents such as chlorates. In 1898 L. The reaction time was rendered by Staudenmaier using sulphuric acid in Brodie's reaction mix. In 1958, in place of chlorate producing toxic gases, Hummers and Offeman reported graphite oxide preparation using potassium permanganate. Vogt studied graphene oxide exfoliation about 90 years after Brodie, and noticed broken sheets using electron microscopy transmission. Boehm et al. named them as "graphene" in 1986. Geim and Novoselov separated a single layer of carbon atoms using scotch tape by mechanical exfoliation and they received the Nobel Prize for their research and researched graphene's electronic properties. Their work set off researchers to study graphene more for different Application. Use graphite as raw material or using any carbon content (methane, ethane, acetylene) will synthesize graphene.

1. The exfoliation method of graphite includes;

- Mechanical cleavage
- Liquid-Phase Exfoliation
- Electrochemical methods.

2. Using Carbon precursor, Chemical Vapor Deposition and Thermal Decomposition of SiC are used.

1.10.1 Chemical Deposition Method

The carbon atom from the hydrocarbon nucleate on the substratum and nuclei expand to

give a larger film in this phase transition metal substratum placed in a closed chamber and slowly heated to 1000 C with the continuous flow of the feed gas.

1.10.2 Thermal decomposition of silicon carbide

This approach employed SiC segregation. This process is capable of producing large graphene films. This process involves two steps; SiC annealing at above 800 ° C under continuous flow of H2 or Argon, which causes Si to sublimate, carbon atoms arrange to give graphene in the second step.

1.10.3 Mechanical cleavage

Mechanical exfoliation is considered the mother of graphene synthesis since Geim used scotch-tape to remove single layer graphite. He stuck graphite on a piece of tape and cleaved it with another sticky tape until invisible powder remained on the starting tape, then moved it to the substratum of silicon dioxide.

1.10.4 Electrochemical method

In this method boro-silicate glass pressed on graphite layer at 200°C, and the voltage of 1700-1800V is applied. The electric field pull the layers of graphite apart and deposited on glass plate.

1.10.5 Exfoliation of Graphite

Exfoliation of graphite is most convenient method to produce graphene. There are two ways of graphene synthesis by this method;

a) Exfoliation of Graphite by using Solvent.

b) Exfoliation of Graphite by Oxidation.

a. Exfoliation of Graphite by using Solvent

Process involves three steps; in the first step the graphite is mixed in a solvent that increase the distance between the graphite layers, in second step mixture is ultra- sonicated to split graphite layer into individual platelets. Final step is the purification of the product by removing solvent.

b. Exfoliation of Graphite by Oxidation

Oxidation route of graphene synthesis by using graphite as starting material is largely used method. Oxidation of graphite is done by using strong oxidizing agent like KMnO4 and concentrated sulfuric acid followed by reduction using strong reducing agent like ascorbic acid or the salts of hydrazine to give graphene usually called reduced graphene oxide (rGO).

1.11 Reduction of GO

During graphite oxidation various functional groups are attached to the sheets of GO. Depending on the type and position these functional groups have different binding energies. To obtain graphene, this functional group should be removed, which is called reduced graphene oxide(rGO) the graphene obtained by removing functional groups from GO. Comprehensive reduction of GO is very difficult to achieve, but graphene output by GO is very attractive for large-scale synthesis and applications. The rGO sheet structure is given in figure.

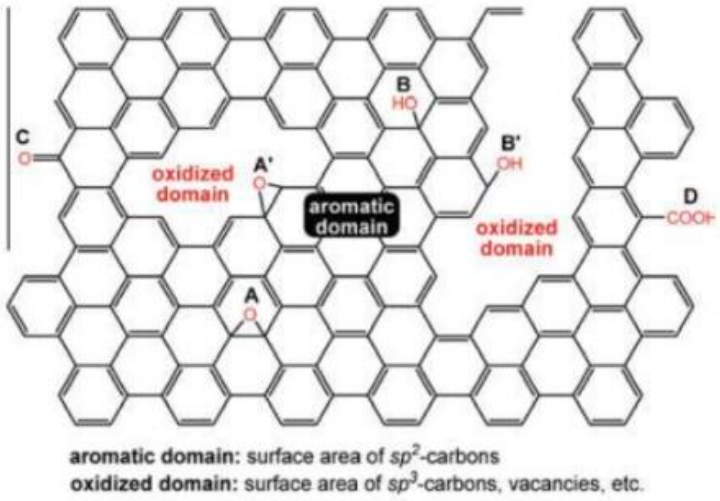

Figure 5: Reduction in graphene

1.12 Graphene Doping

Heteroatom doping is the perfect way to regulate the graphene's semiconducting properties. Nitrogen atom is a natural heteroatom for doping due to similar properties. Various methods

of nitrogen doping may yield different properties. There are many methods of synthesis available as shown below;

1. Chemical Vapor Deposition(CVD)
2. Thermal Annealing
3. Pyrolysis
4. Solvothermal
5. Method
6. Arc-Discharge
7. Plasma Treatment
8. N2H4 Treatment
9. Hydrothermal Method
10. Wet Chemical Synthesis

Graphene doping with nitrogen produced different kinds of groups in lattice as shown Pyridinic, Quaternary and Pyrrolic.

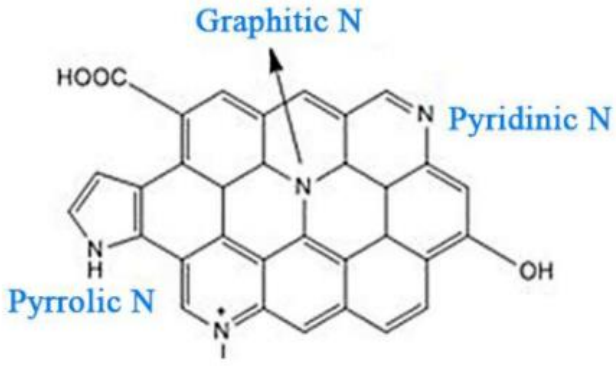

Figure 6: Doping of graphene

1.13 Sensing Mechanism

A general sensing mechanism involves the combination of physisorbed gas with oxygen, which is chemisorbed on the sensing material surface.

As oxygen chemisorbed on the surface it forms many ions as shown below:

$$O_2\,(gas) \leftrightarrow O_2\,(ad) \leftrightarrow O_2^-\,(ad) \leftrightarrow O^-\,(ad) \leftrightarrow O^{2-}\,(ad) \leftrightarrow O^{2-}\,(lattice)$$

For Methane gas, sensing mechanism would be:

$$2O_2^-(\text{adsorbed}) + CH_4 \rightarrow CO_2 + 2H_2O + 2e(\text{shared by sensing material}) \quad (3)$$

$$4O^-(\text{adsorbed}) + CH_4 \rightarrow CO_2 + 2H_2O + 4e(\text{shared by sensing material}) \quad (4)$$

CH4 release electrons on interactions and cause a decrease in resistance of the overall material. The doped graphene or reduced graphene in composite provide energetically favorable sites and increase the sensitivity.

CHAPTER 2

LITERATURE REVIEW

2.1 Methane Gas Sensors

The first industrial-age gas detector was the fire safety lamp (or Davy lamp) invented by Sir Humphry Davy (from England) in 1815 to detect the presence of methane (firedamp) in underground coal mines. The fire safety lamp consisted of an oil flame in fresh air which was adjusted to specific height. Inside a glass sleeve with a mesh flame arrestor was placed to avoid ignition with the flame of the lamps. The height of the flames differed according to the presence of methane (higher) or the absence of oxygen (lower). To this day, safety lamps are still in use in some parts of the world.

The modern era of gas detection began in 1926-1927 with Dr. Oliver Johnson designing the catalytic combustion (LEL) sensor.

In 1928 Dr Oliver Johnston and Phil Williams founded the world's first gas detection company, Johnson-Williams Instruments (or J-W Instruments) in Palo Alto, CA. J-W Instruments is known for being Silicon Valley's first electronics company. J-W Instruments pioneered many "firsts" in the modern age of gas detection over the next 40 years, including making instruments smaller and more compact, creating a portable oxygen detector, as well as the first hybrid device capable of detecting both combustible gasses / vapors and oxygen.

The 1990s saw the launch of metal-oxide-semiconductor sensors (MOS sensors). G proved the earliest known MOS gas sensor known. G. Faglia, S. Groppelli, P. Nelli and A. Sberveglieri. Camanzi was founded in 1990. Since then MOS sensors have become effective detectors of environmental gases.

The electrochemical sensors are highly accurate, they work at room temperature but have a complex structure, high cost and short lifetime. Due to simplicity, low cost and a wide range of applications CH4 chemi-resistive sensor is under considerable interest. Efforts are underway to establish sensing material that increases chemi-resistive sensor sensitivity and

operates at room temperature.

The use of material for solid-state gas sensors is not limited. A sensor should be generally highly sensitive, selective and stable. Graphene is known to be "the next wonderful material" the electron mobility in graphene is about 100 times greater than any other conductive material and it has the ability to tolerate high electrical current concentrations. Graphene is completely impermeable to all gasses, and has a high capacity for adsorption. These two properties are of great value in the application of gas sensing.

Figure 7: Gas sensor

2.2 Graphene for Methane Gas Sensor

When there are electrical or thermal failures, such as oil or high-temperature overheating, partial discharge, spark discharge, or arc discharge, the hydrocarbon gas CH4 may be produced. Such four hydrocarbon gases have a small difference in molecular structure and chemical composition, and they are usually similar to the sensing materials. According to the relationship between the main gases and associated types of fault (Bakar et al., 2014), when the oil-immersed equipment suffers from an electrical or heating failure under any circumstances, the emitted hydrocarbon fault gas is primarily CH4 or C2H2 and the quantity of each is greater than the high molecular weight gasses (C2H4 and C2H6) (Sun et al., 2017). Moreover, the detection of CH4 is becoming more and more important in many fields as the mining industry, environmental monitoring and petrochemical industry.

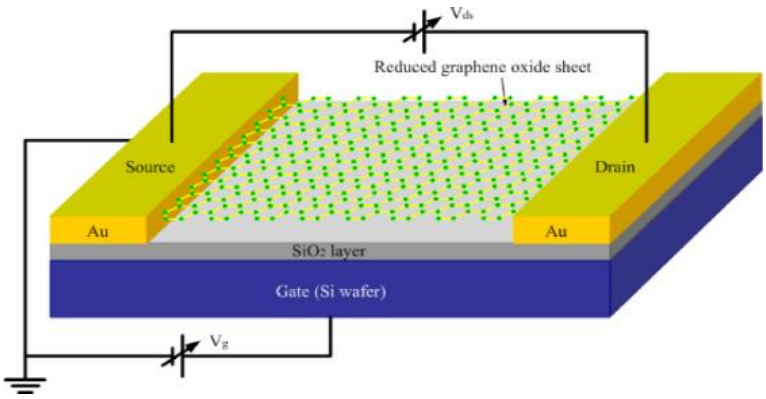

Figure 8: Graphene synthesis

Hence, research into the detection of hydrocarbon gas in oil-immersed equipment is focused primarily on CH4. Wu et al. identified a polyaniline (PANI) / graphene-based CH4 sensor. This sensor showed a high sensitivity of 10–3,200 μL / L at room temperature, due to the existence of the PANI / graphene π* conjugation system (Wu et al, 2013). Zhang et al. (2016) prepared hybrid NiO / rGO materials and showed a high selectivity against CH4 toward H2, CO and CO2. At 260 ° C, the answer to CH4 100 μL / L was 2.2 per cent. Graphene hybrid with ZnO (Zhang et al., 2015b) and SnO2 (Navazani et al., 2018) also showed unusual sensing properties at about 190 and 150 ° C at CH4. At room temperature, Nasr Esfahani et al. (2017) synthesized Pd-doped SnO2/rGO via hydrothermal path, and sensing output to 800–16,000 μL / L CH4. The p-n heterojunctions between SnO2 and rGO, functional oxygen groups, and high specific surface area of hybrid SnO2/rGO materials lead to good sensor efficiency (Jin et al., 2016). In addition, hybrid materials were synthesized with Ag / ZnO /rGO (Uddin et al., 2015b) and Ag / SnO2/rGO (Jiang et al., 2017), and sensors were developed for low-temperature CH4 sensing. However, with the decrease of operating temperature, the sensitivity of the sensor was reduced with longer response-recovery time.

Table 1: Literature on graphene sensor

GAS	HYBRID MATERIAL	TEMP C	DETECTION RANGE (□L/L)	CONC. (□L/L)	RESPONSE TYPE	SENSOR RESPOSE	τ(res)/τ(rec) (s/s)	reference
CH4	PANI/rGO	RT	10-3200	100	Rair/Rgas	~3	85/45	Wu et al.,2013
	NiO/rGO	260	100-6000	100	ΔR/Rair	~2.2%	6/16	Zhang et al., 2016
	ZnO/rGO	190	100-4000	1000	ΔR/Rair	~12%	~200	Zhang et al., 2015b
	SnO2/rGO	150	1000-10000	1000	ΔR/Rair	47.6%	61/330	Navazani et al., 2018
	Pd/SnO2/rGO	RT	800-16000	14000	ΔR/Rair	9.8%	5/7 min	Nasresfashani et al, 2017

2.3 Graphene and Metal oxide Composites for CH4 Sensing

Until now, metal oxide based gas sensors based on nanoparticles have been largely investigated. Metal oxides are well known to alter their electrical resistance with the alteration in gas composition in the environment. Taguchi developed commercially gas sensor for the sensing of explosive gases in 1968. The sensor was designed for chemical sensing using SnO2 thick film, Other than SnO2, TiO2, In2O3, WO3, ZnO, Fe2O3, etc.

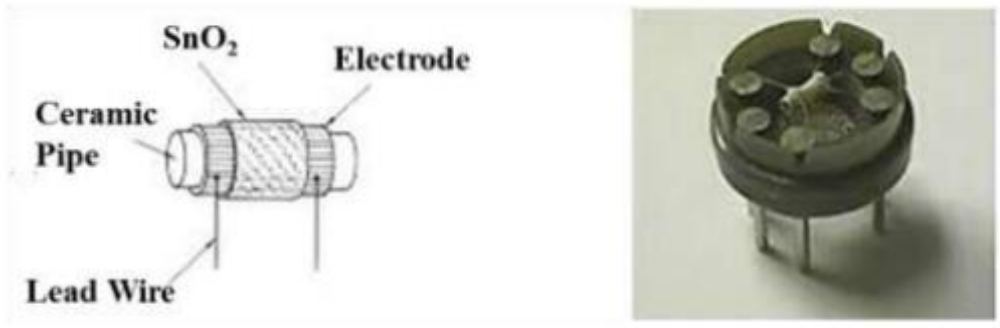

Figure 9: Metal oxide sensor

In addition, composites of noble metals with metal oxides have been tested to improve resilience and stability. Yamazoe, reported most significant findings in 1991. He proved that the efficiency of the sensor is greatly increased with the reduction in crystallite thickness. With the invention of metal oxide nanowires the metal oxide gas sensor took a new turn. It shifted the research community to synthesize various formed metal oxide nanoparticles for gas sensors. RGO / Metal Oxide Nano composite has shown great potential for next-generation metal oxide gas sensors with high stability, long service life and low operating temperature or functionality, Unchanged from the original MOF topology. The transition metal ions to the organic ligands give coordination positions. Ligands are typically multi-dented bridging linkers, providing a wide choice of connecting sites, they have organic linker direction and binding power, exceptional to their topology. Rigid ligands will be responsible for the synthesis of the physical topologies.

2.4 Graphene and MOFs Composites for CH4 Sensing

Metal-organic frameworks (MOFs) are porous polymer coordinators with exceptional properties such as permanent Nano scale porosity with extraordinary surface area, uniform and tunable pore size, and functional capability. Such properties strengthen them over traditional porous materials. MOFs are used extensively in gas storage, separation, catalysis, and chemical sensors under intensive study. MOFs are typically synthesized by the use of coordination bonds to compile metals and multi-dentate organic linkers. Many MOFs have a 3-dimensional structure which integrates different pores and several open channels. MOFs are formed by a complex metal ion coordination reaction and organic bonding. MOFs

network structure relies heavily on the properties of the organic ligands and the coordination of metals. In particular, new MOFs can be set up by modifying the linker bridge or its functionality, without altering the MOF's original topology. The transition metal ions to the organic ligands give coordination positions. Ligands are typically multi-dented bridging linkers, providing a wide choice of connecting sites, they have organic linker direction and binding power, exceptional to their topology. Rigid ligands will be responsible for the synthesis of the physical topologies.

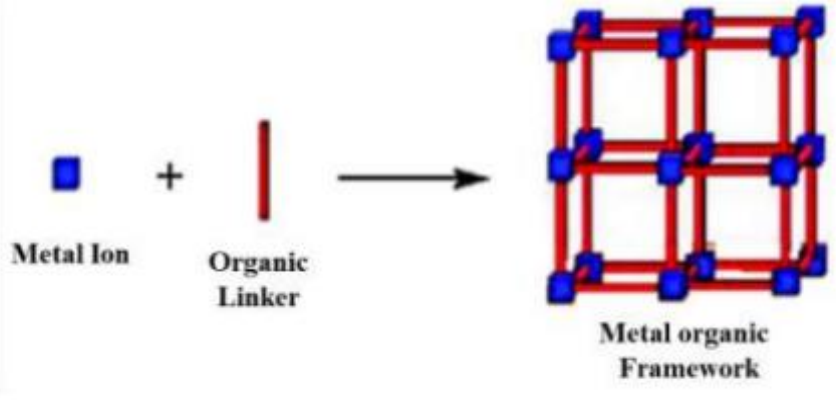

Figure 10: MOX Linkages

Numerous methods can be used to synthesize MOFs, including hydrothermal, room temperature crystallization, solvo-thermal, and microwave heating, vapor diffusion, direct mixing and so on. The methods of solvo-thermal and room temperature synthesis are commonly used for the processing of MOFs. These routes of synthesis also tend to lead to differing MOF properties. For example, solvo-thermal synthesized MOFs have a larger particle size than the synthesis method for room temperature.

2.5 Graphene Decorated with Silver Nanoparticles for Methane Gas Sensor

An experiment on graphene (G), decorated with silver nanoparticles (AgNPs), methane sensing properties under ambient conditions. To do so, we first implement an important

change to the standard way AgNPs decorate graphene. From the structural product analysis (AgNPs / G), it is concluded that graphene is actually decorated with a uniform distribution by AgNPs free of aggregation. Then, as a resistivity-based sensor, the so-produced material is used to examine its response to methane gas present. Our experiments are carried out at relatively low temperatures, for different concentrations of silver-to-graphene mass (SGMRs) and methane. We also made the calculations, at room temperature, for different levels of humidity to compensate for the effects of humidity. Our results show that an improvement in SGMR increases AgNPs / G's response to methane with an optimal SGMR value of 12%. It is also shown that, even at room temperature, maximum response increases linearly and rapidly for methane concentrations less than 2000 ppm. In addition, we demonstrate that AgNPs / G is reproducible for methane sensing with a low detection limit, highly stable, sensitive, reversible, repeatable, and sensor to sensor. The results thus promise a low-cost and simple-to-fabricate methane sensing device.

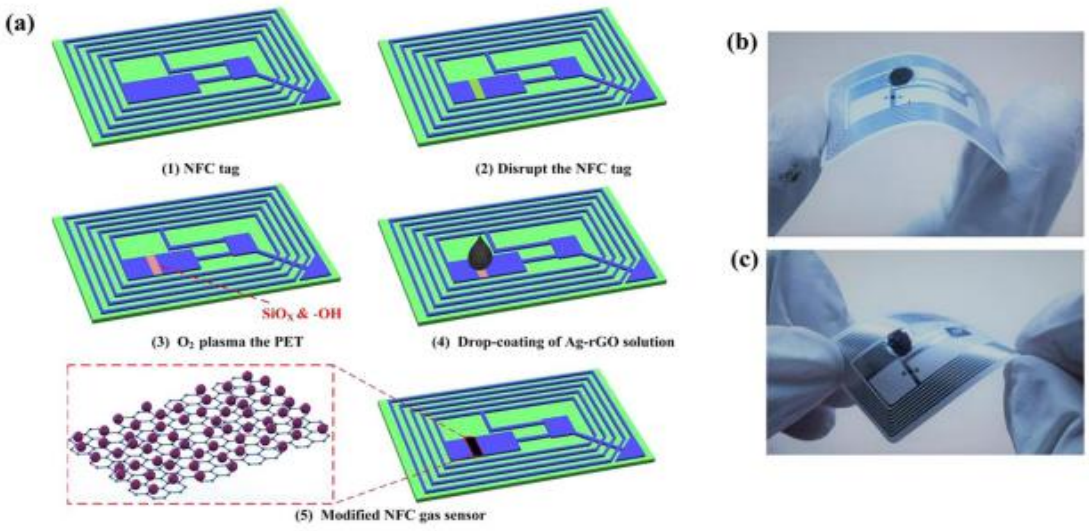

Figure 11: Silicon substrate

2.6 Mechanism of Methane Gas Sensing by the proposed material

In this section we discuss the physical reasons for AgNPs / G's response to the presence of CH4, as predicted and characterized in the sections below. First of all, when atmospheric oxygen molecules are adsorbed by graphene, the π-electrons move from graphene to O2 or O, shifting the hybridization of carbon atoms from sp2 to sp3

$$O_2(\text{adsorbed}) + e(\text{from sensing material}) \rightarrow O_2^-(\text{adsorbed}) \quad (1)$$

$$O_2^-(\text{adsorbed}) + e(\text{from sensing material}) \rightarrow 2O^-(\text{adsorbed}) \quad (2)$$

Although both processes result in ionized oxygen, the former predominates at low temperatures (< 100 ° C), while the latter mainly occurs at higher temperatures. The accumulation of negative charges around ionized oxygen, followed by the depletion of negative charges in graphene, results in an induced electric dipole. In addition, the local electric dipoles transform the sheet of graphene from a gapless semiconductor into a gapped p-type one.

When AgNPs are added, the p-type character of G+O2 is conjectured to rise. This conjecture is based on the fact that the work function value corresponding to G + O2 is smaller than that of AgNPs + O2. Thus electrons move from G + O2 to AgNPs + O2 when the two touch each other. Such a process occurs until the Fermi energies (working functions) align themselves. As a result, when Ag nanoparticles are introduced in the vicinity, the accumulation of holes in graphene becomes greater.

$$2O_2^-(\text{adsorbed}) + CH_4 \rightarrow CO_2 + 2H_2O + 2e(\text{shared by sensing material}) \quad (3)$$

$$4O^-(\text{adsorbed}) + CH_4 \rightarrow CO_2 + 2H_2O + 4e(\text{shared by sensing material}) \quad (4)$$

This argument is helpful when detecting gases that are either electron-acceptor or electron-donating. However, we should point out that direct transfer (physisorption) of electrons from CH4 occurs at low temperatures, with less charge transfer capacity. On the other hand, at higher temperatures a higher transfer of charge occurs mainly by gas oxidation (chemisorption).

CHAPTER 3

EXPERIMENTAL SYNTHESIS

3.1 Synthesis of Exfoliated Graphite Oxide (XGO)

Materials: Graphite, distilled water

Procedure: Aqueous colloids of XGO were prepared by dispersing 1.0 g GO into 500 mL of distilled water by ultra-sonication and centrifugation for 2 hr. to remove any un-exfoliated GO. The XGO was dried at 45°C for 24 h.

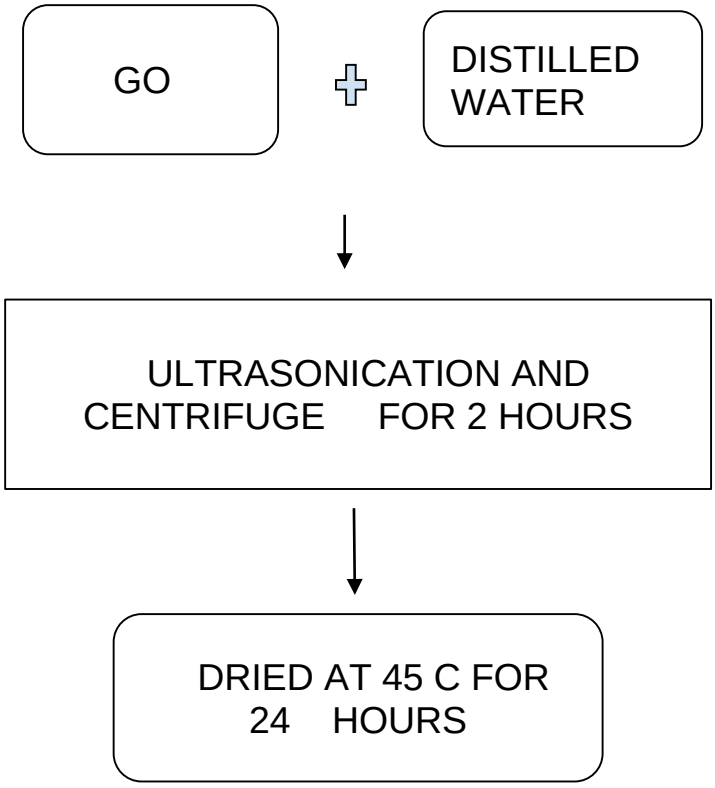

Figure 12: synthesis of GO

3.2 Preparation of graphene oxide by a modified Hummer's method

By improving the work of Brodie and Staudenmaier, Hummers identified a novel method of graphite oxidation in 1958, most commonly used in these days. In Hummer's process KMnO4 and-1O3 oxidized graphite to graphene oxide in the presence of H2SO4. Nevertheless, this procedure has some disadvantages, NOx release and Na+ and NO3-Ion presence. In 2010, by increasing the amount of H2SO4, James M. Tour improved the Hummer's process and eliminated the ions from the oxidation reaction, rendering the reaction non-explosive while increasing the reaction time and high oxidant consumption. Many changes were made to increase the yield of the process Hummer used to increase yield. A novel adapted method of the Hummer is used for GO synthesis in this work.

Material: Graphite powder, Sulphuric acid (97%), Phosphoric acid H3PO4 (87%), Potassium Permanganate (KMnO4), NaNO3, Hydrochloric acid (HCl 35%), H2O2 (30%) acquired from Sigma Aldrich & Ethanol (≥99.5 %.) from MERCK. All reactants and solvents have been used without further purification.

Procedure: The mixture of flake graphite/NaNO3 was prepared in weight ratio of 2: 1. The mixture was added into a beaker with a certain amount of 98 wt. % H2SO4 at 15°C and phosphoric acid where a suspension is obtained. Then, KMnO4 powder which acted as an oxidation agent was gradually added into the suspension with continuous stirring. The weight of the KMnO4 powder is 3 times as much as the one of the mixtures.

Figure 13: Thin film of GO

There were 3 steps for the following process. First of all, it is the low temperature reaction. The temperature of the mixture was controlled below 20°C for 2 hours; at the same time, the suspension should be stirred continuously. The second step is the mid temperature reaction. The temperature of the mixture was maintained at 35°C for 30 minutes after KMnO4 was totally dissolved. Finally, it is the high temperature reaction. A certain amount of deionized water was added into the mixture slowly; therefore a large amount of heat was released when concentrated H2SO4 was diluted. 15 minutes later, certain amounts of hot water and 30% H2O2 aqueous were added into the mixture, respectively, with continuously stirring.

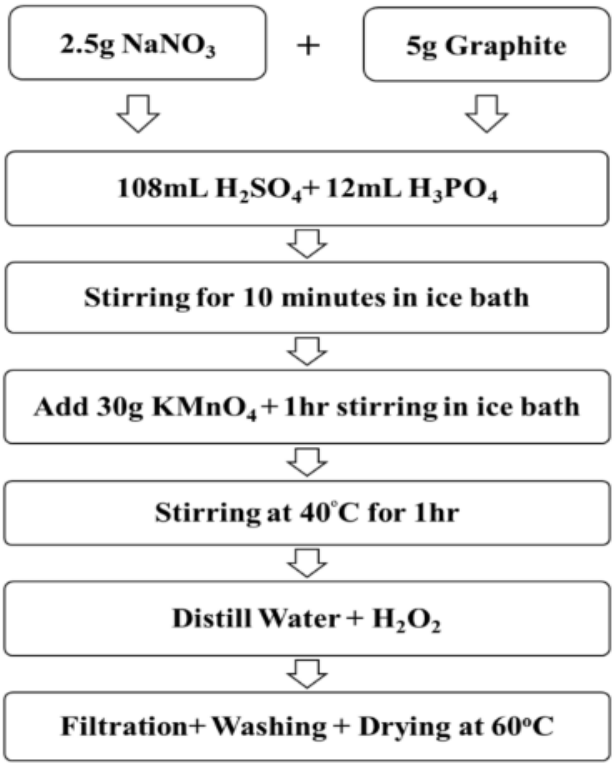

Figure 14: Synthesis of GO

3.2.1 Mechanism of Hummers

In modified hummer's method, though KMnO4 is used as a kind of oxidizing agent. Dreyer et al. Believed that the active species was Mn2O7. The following equation gives the reaction

between KMnO4 and H2SO4

$$KMnO_4 + 3H_2SO_4 \longrightarrow K^+ + MnO_3^+ + H_3O^+ + 3HSO_4^- \quad (1)$$
$$MnO_3^+ + MnO_4^- \longrightarrow Mn_2O_7$$

The edge of graphite was oxidized in low temperature reaction and intercalated with the aid of the oxidizing agent. During that process –OH was created. The oxidation capacity also improves in the mid-temperature reaction, with the increase of temperature. In this process, more functional groups of oxygen are formed, and the oxidizing agent penetrates into the internal graphite layer; hence, this process leads to an increase in spacing. During the watering process concentrated H2SO4 releases a large amount of heat in the high temperature reaction. There is a loss of force between layers and eventually the GO could be completely exfoliated to single layers.

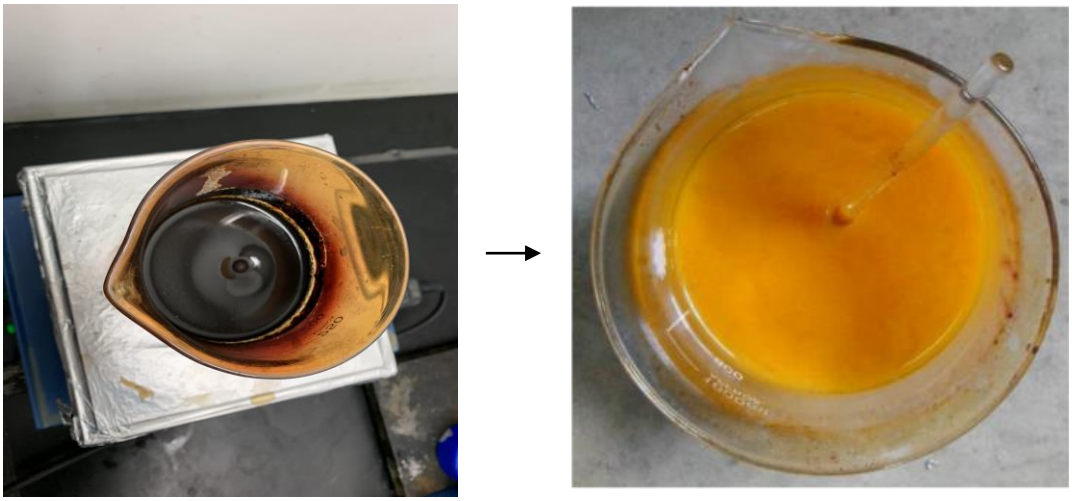

Figure 15: Washing of GO

3.3 Synthesis of rGO

Material: GO powder (prepared by above Method), L-Ascorbic Acid, N,N-dimethylformamide (DMF) and Ammonia Solution (25%) bought from Sigma- Aldrich with best quality assurance and were used without further processing.

Procedure:

400 mg GO was dispersed in 400 mL water by means of 30 minutes' ultrasonic treatment. As a result, a homogeneous brown GO aqueous suspension was obtained. The pH of the suspension was adjusted to 10 by dropping NH3H2O. A mount of hydrazine hydrate was added into suspension and heated at 80°C for 24 hours, and the weight ratio of hydrazine hydrate and GO was controlled at 10: 7. A kind of black flocculent substance was gradually precipitated out of the solution. The product was obtained by filtered with the qualitative filter paper. Finally, the resulting black product was washed with methanol and water and dried at 80°C for 24 h.

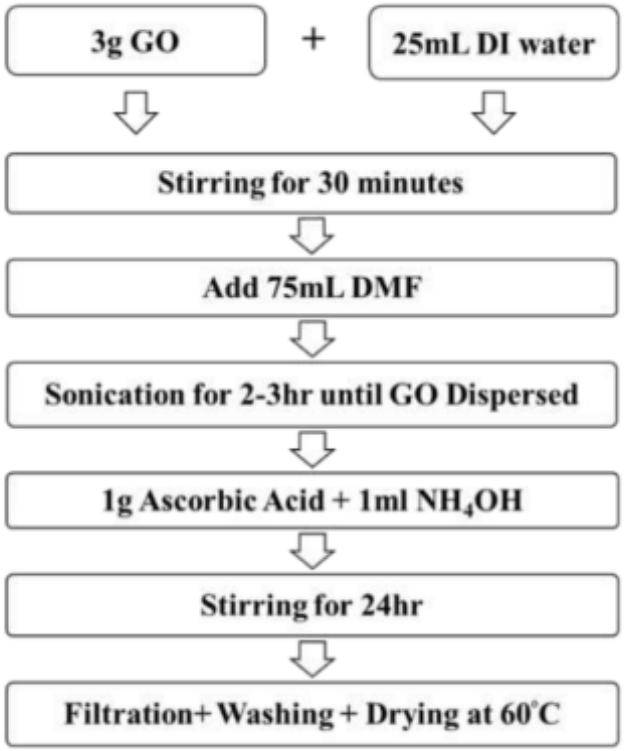

Figure 16: synthesis of rGO

3.4 Synthesis of Ag nanoparticles

Materials: The starting precursors for synthesis are Silver Nitrate, propanal and diethyl amine.

Procedure: Aqueous solutions with different concentrations of silver nitrate and propanal were mixed together in a calculated volume of deionized water having TDS (total dissolved solid) of 0~5mgs/liter by mixing through magnetic stirrer until the solution became homogenized. A pre calculated milli molar aqueous solution of diethylamine (DEA) was added to it quickly and stirred vigorously (Conc. of chemical used in synthesis procedure mentioned in the Table). The color change in the solution is observed after 10 to 20 minutes, from black to brown and then finally a dark gray colored higher concentrated Silver Nitrate precipitates were obtained and a yellowish-green colored suspension was obtained for lower concentration of silver nitrate. The experiment was repeated with argon environment of 0.1~0.2 atm, in a glove box to homogenize the solution and observed that cluster of particles suspended in a solution. After filtering the mixture and washing the residue repeatedly 2 to 3 times with distilled water, the residue was collected and dried in a vacuum furnace at 50°–60°C.

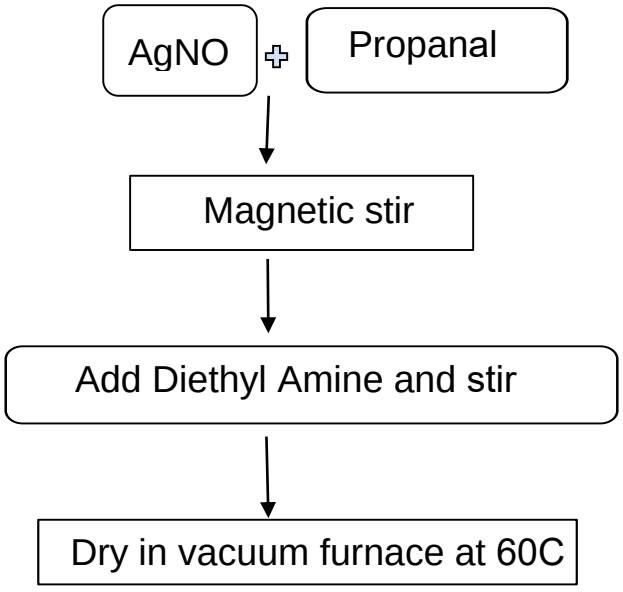

Figure 17: Synthesis of AgNP

This experiment was composed of 2 stages. In the first stage all the mixing of precursors was at 30 ° C at the laboratory's ambient conditions by simply stirring the solution at 20~30 RPM & in the second stage a controlled environment is provided in the glove box by maintaining the inside working pressure & argon gas jet is provided to homogenize and stabilize the particle by removing the oxygen trapped in the solution. The table shows the physical structure of the setup:

Table 2: Mean sizes of AgNP

Sr No.	Conc. AgNO3 (mM)	Conc. propanal (mM)	Conc. DEA (mM)	Particle size(+-10nm)	Mean (nm)
1	150	60	80	350-300	325
2	150	60	80	325-275	300
3	100	50	85	300-250	275
4	100	50	90	300-225	260
5	75	45	100	200-150	175
6	75	40	100	200-150	175
7	50	40	120	150-100	125
8	50	35	120	150-70	110

The concentration of AgNO3 & DEA has an inverse relation between them. When the concentration of AgNO3 goes on increasing & the concentration of DEA goes of decreasing the outcome is large particles size with wide distribution & vice versa.

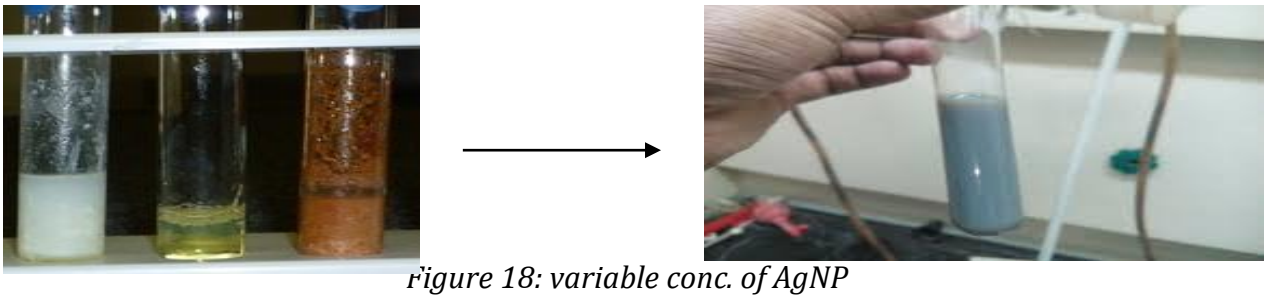

Figure 18: variable conc. of AgNP

3.5 Conclusion for synthesis of GO and rGO

GO was prepared using Hummers ' method and rGO was successfully prepared with the aid of aqueous NH3H2O and hydrazine hydrate. The findings of the analysis show that the graphite oxide layer spacing was longer than that of graphite. The graphite crystal structure was changed. Graphite was oxidized to GO, and the GO found lots of oxygen-containing groups. Typical fold morphologies have been found both on the rGO surface and bottom.

Hummers ' method can synthesize GO on a large scale compared to the traditional CVD method, then rGO can be prepared with the aid of a reducing agent, and this step costs a little bit. In the meantime, the prepared GO is quickly distributed in solution. The GO modification is easy in this case and is suitable for GO application in composites and energy storage devices.

3.6 Characterization

Synthesized materials characterized by following characterization techniques:

3.6.1. XRD Analysis

XRD (AXS partnership, Germany) has obtained crystal characteristics of flake graphite, GO, and rGO, with a scan speed of 4 ° /min from 5 to 60 ° angles. With the support of Bragg equation, the layer spacing (spacing) could be determined, and the increase in the diffraction peak could also be observed.

XRD is a feasible method for calculating crystal dimensions. Diffraction of X-rays from

different planes is recorded in this technique, and a pattern of diffraction is obtained following Bragg's equation.

In diffraction pattern the intensity depend on numbers of X-ray diffracted at particular angle 2θ, current and voltage of the X-ray source.

The position of peak in pattern defines the crystal configuration and helps to identify material. Figure describes the working principle of XRD equipment.

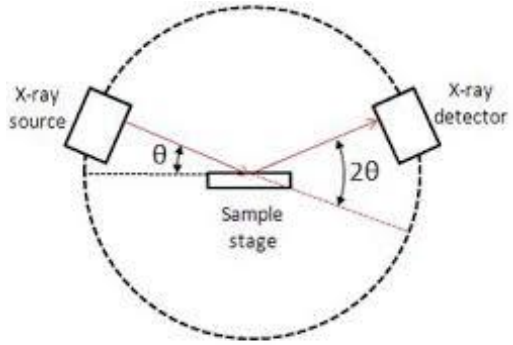

Figure 19: XRD characterization

3.6.2. SEM Analysis

SEM is the most commonly used to study material morphology, structure, and tiny details. In SEM high-energy electron beam is mounted on the surface of the specimen. In combination with secondary electrons the backscattered electrons form a picture. Backscattering electrons gives material phase distinction, and secondary electrons provide information on topography and morphology. The creation of X-rays happens also with the interaction of electrons with sample atomic electrons. The SEM machine's function is explained in the figure

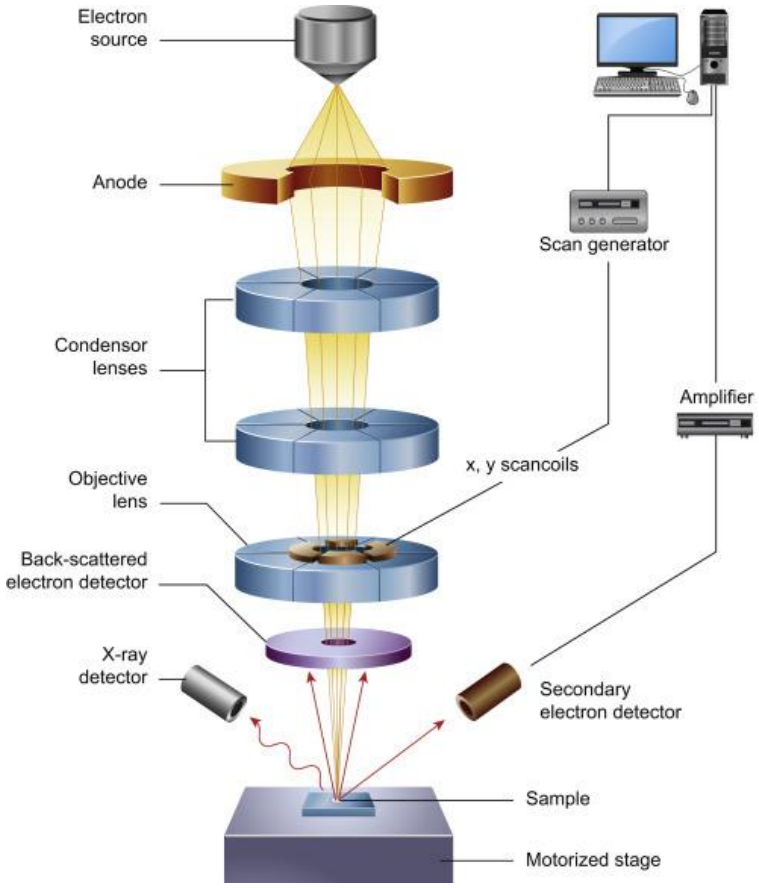

Figure 20: SEM characterization

The micromorphology of rGO was observed by SEM (JSM-6700F, Japan), with the acceleration voltage from 0.5 to 30 KV.

3.6.3. FTIR Analysis

IR is a vibrational spectroscopy used to identify the type of functional groups present in a material and the type of bonds. To obtain bandwidth, the Fourier Transformation (a mathematical procedure) is used.

The covalent bonds are not rigid, and either stretch or bend in vibrational motion. Infrarot radiation absorption affects the vibration status of the bonds and creates a spectrum.

Spectra of dried GO and rGO were obtained by Tensor 27 FTIR-ATR (Bruker corporation, Germany), with the resolution of 4 cm−1 from 3700 to 500 cm−1 spectral region, and

functional groups of GO and rGO can be observed.

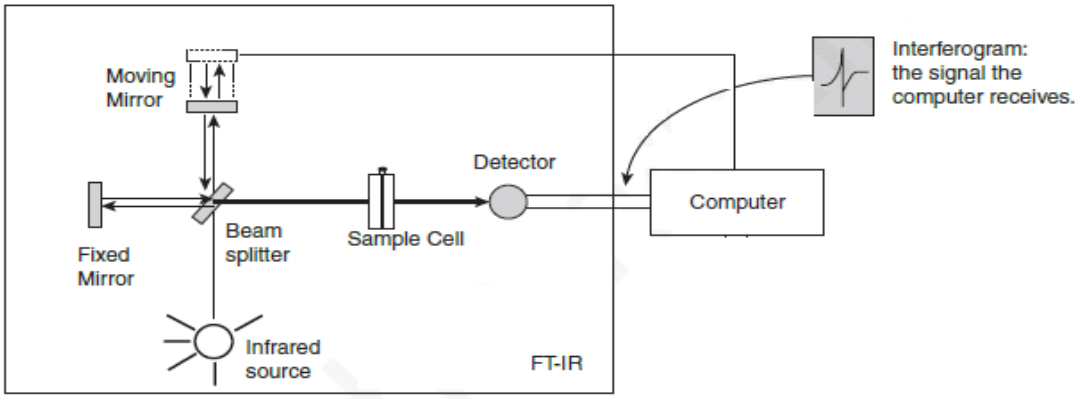

Figure 21: FTIR Characterization

3.6.4 UV Analysis

UV-Vis Spectroscopy (or Spectrophotometry) is a quantitative method used to measure how much light is absorbed by a chemical substance. Spectrophotometry is a quantitative measure of the absorption / transmission or reflection as a function of the wavelength of a material. Despite being called UV-Vis, the typically used wavelength range in the near-infrared ranges from 190 nm to 1,100 nm.

Simply by studying the number of photons (light intensity) that reach the detector, we can determine the amount (or concentration) of a known chemical substance by using a spectrophotometer and performing absorption / transmission measures. The more light a substance absorbs at a given wavelength, the higher the known concentration.

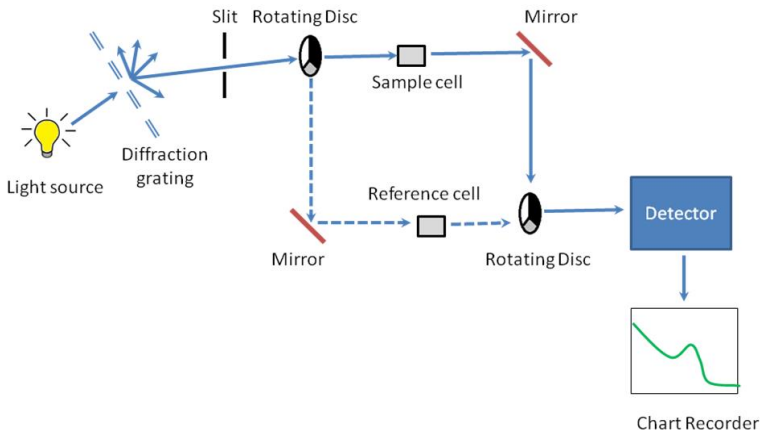

Figure 22: UV Characterization

3.6.5 TGA Analysis

Thermo gravimetric analysis or gravimetric thermal analysis is a thermal analysis process in which the mass of a sample is determined over time as the temperature changes. This calculation provides information on physical phenomena such as phase transitions, absorption, adsorption, and desorption; as well as chemical phenomena such as chemisorption, thermal decomposition, and reactions to solid gases (e.g., oxidation or reduction).

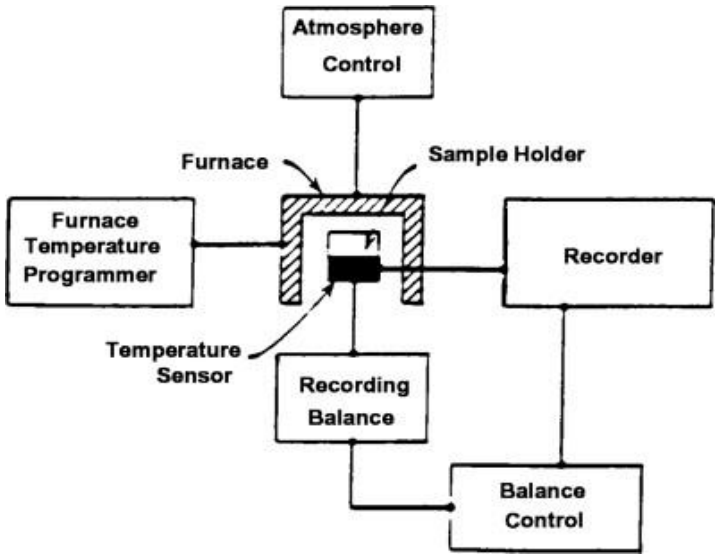

Figure 23: TGA instrumentation

3.6.7 Elemental Analysis

Energy Dispersive X-Ray Analysis (EDX), known as EDS or EDAX, is an x-ray method used to classify the elementary material composition. EDX systems are attachments to instruments for electron microscopy (Scanning Electron Microscopy (SEM) or Transmission Electron Microscopy (TEM)) where the microscope's imaging capability recognizes the specimen of interest. The data generated by the EDX analysis consists of spectra showing peaks corresponding to the elements that make up the sample's true composition to be analyzed. Elemental mapping of a sample and an analysis of the image are also possible.

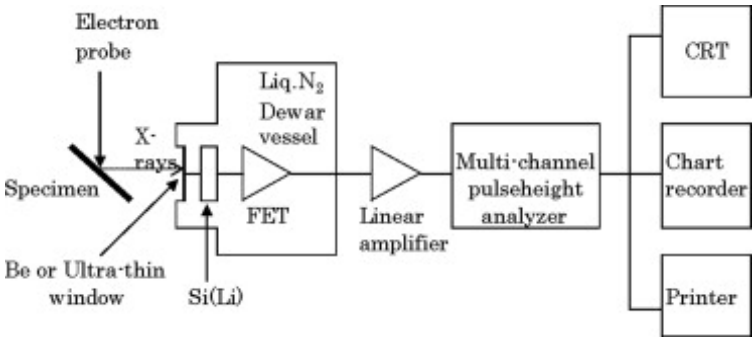

Figure 24: Elemental Analysis Instrumentation

3.6.8 Particle Analyzer

Particle size analyzer set the standard for providing fast, accurate distributions of particle size for both wet and dry dispersions. From evaluating product uniformity and solubility to optimizing packaging density to improving final product performance and controlling the flow of powders to increase production efficiency, Analysis of particle size is critical to understanding and controlling a wide array of properties. Distribution of particle size is a unique property for powders, and is an important physical property for determining powder behavior and nature. For this reason the distribution of particle size has to be measured while handling powders.

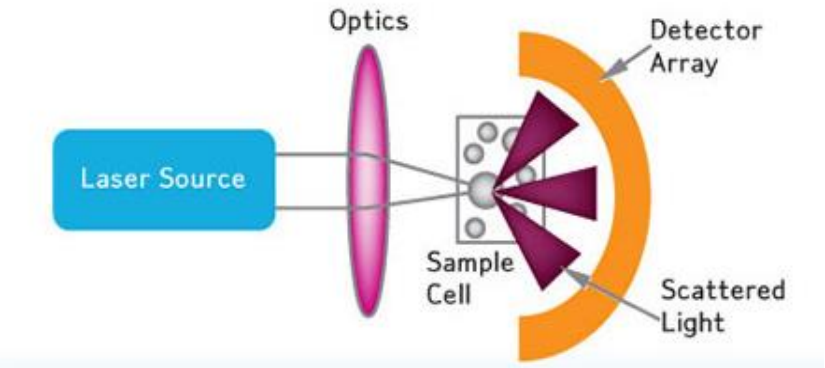

Figure 25: Particle analyzer instrumentation

CHAPTER 4

RESULTS AND DISCUSSIONS

4.1 Result Analysis for exfoliated GO

4.1.2 SEM analysis for XGO

SEM pictures for exfoliated GO shows formation of edgy graphene. It shows the morphology of GO with a layered structure.

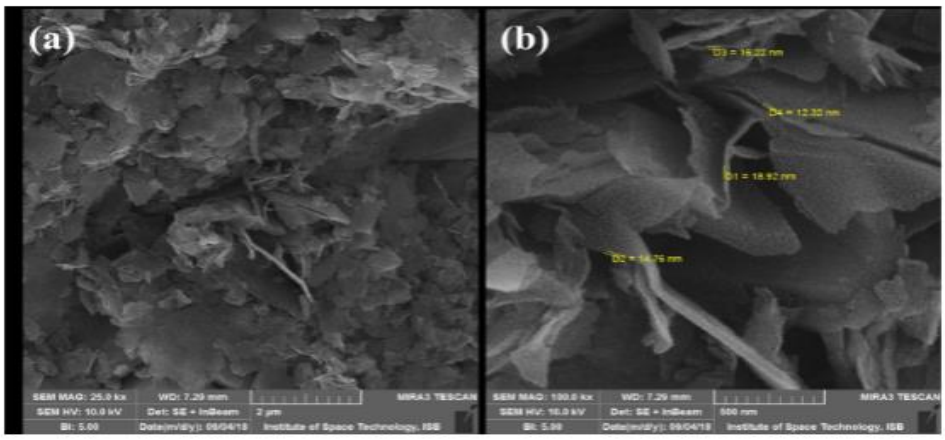

Figure 26: SEM of XGO

4.1.2 XRD for exfoliated GO

XRD peak for exfoliated GO for (002) occurs between 2θ=20-30, whereas weak peaks for (101), (004) and (110) occur at 2θ= 45, 55 and 78 respectively.

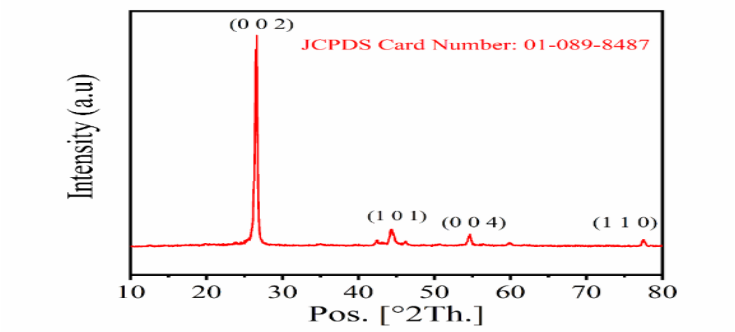

Figure 27: XRD of XGO

4.2 Analysis for GO

4.2.1 SEM Analysis for GO

SEM shows morphology of GO with a layered structure. The epigenetic graphite showed in the presence of strong oxidizing agents KMnO4 and H2SO4. These oxidizing agents concentrate into graphite layer and create oxygen containing functional groups on edges and basal planes, resulting in formation of GO. The GO planes get wrinkled after oxidation in harsh acidic environment. A typical wrinkled image of GO can be seen below

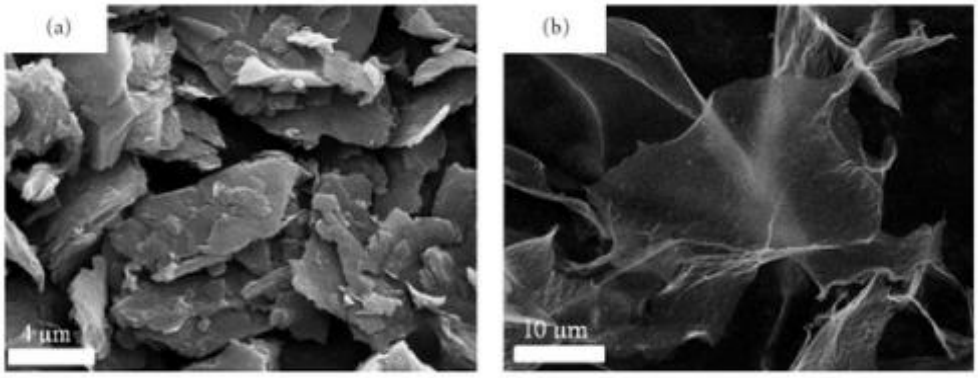

Figure 28: SEM of GO

4.2.2 XRD Analysis Results for GO

Using XRD study, the average crystalline properties of the GO sheet were calculated. See Figure 2(a) for the analysis. The prepared GO sheet showed a very strong peak at 2θ= 10.2 °, in good agreement with the literature surveys. XRD's findings initially proved GO sheet's positive synthesis.

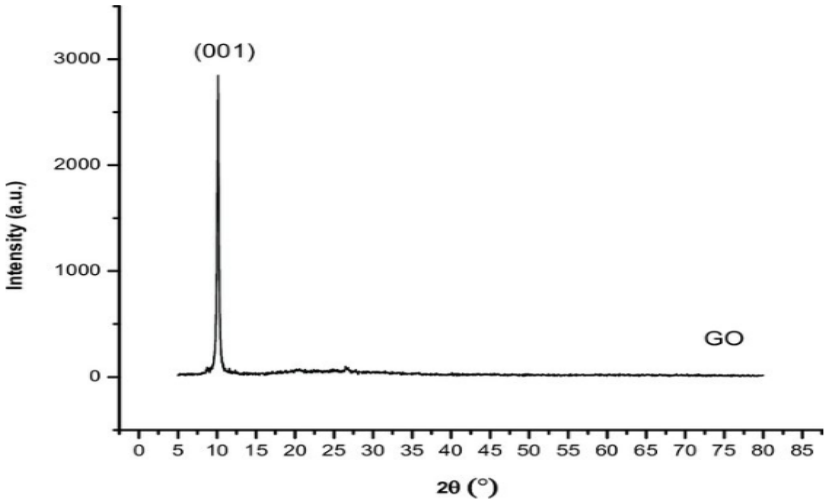

Figure 29: xrd of GO

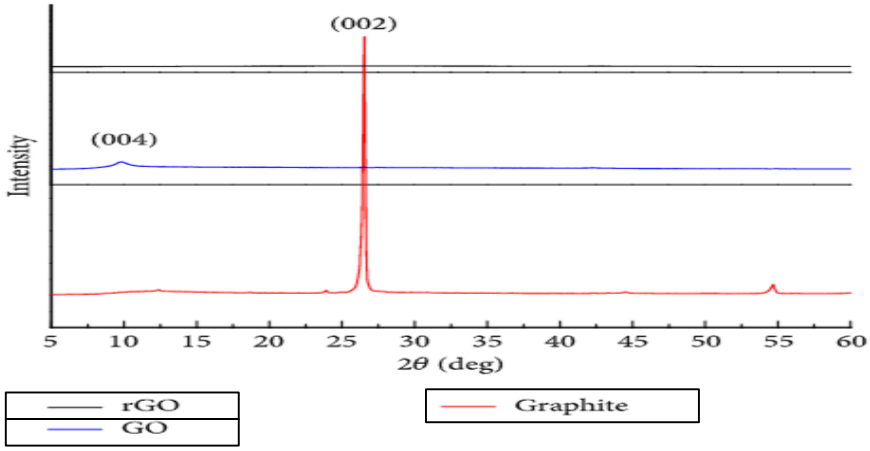

Figure 30: Xrd of GO, rGO, Graphite

4.2.3 FTIR FOR GO

Analysis of FTIR spectra was carried out to investigate the structure and functional groups of the materials, as shown in Figure (b). For carboxyl C= O (1723 cm−1), aromatic C= C (1621cm−1), epoxy C–O (1220 cm−1), alkoxy C –O (1043 cm−1), and hydroxy –OH (3391 cm−1), the GO sheet displayed clear adsorption bands. The presence of functional groups

containing oxygen, such as C = O and C – O, further verified that the graphite was indeed oxidized into GO and conformed to the literature. The analysis of C = C groups revealed that even graphite had been oxidized into GO; the main layer graphite structure has still been preserved. The results of XRD and FT-IR synthesis further demonstrated the successful synthesis of GO sheet.

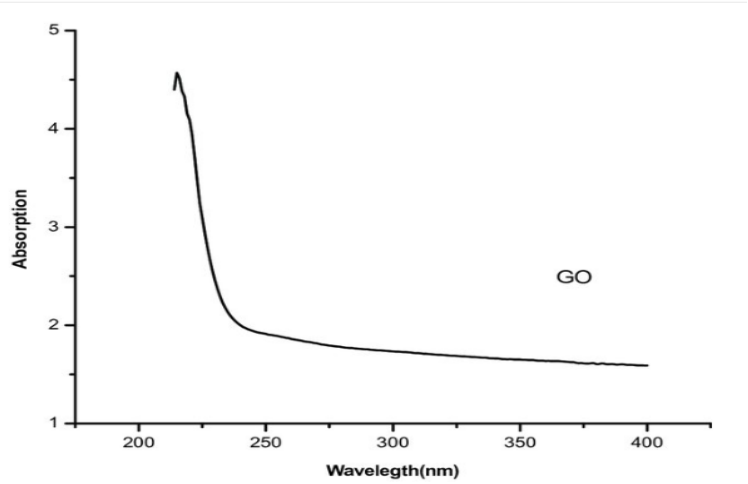

Figure 31: FTIR of GO

4.2.4 The Optical Absorption Properties of GO Sheet

The study of the GO sheet's UV-VIS diffuse reflection spectrum was shown in Figure.

Graphene oxide has been shown to have strong absorption in the visible range (380~800 nm) but absorption in the ultraviolet range has also been slightly reduced..

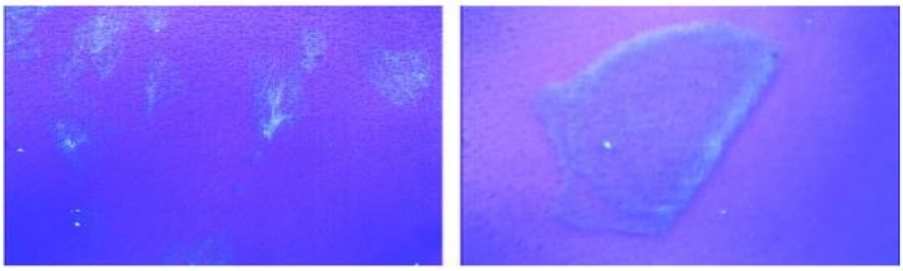

Figure 32: Optical image of GO

The results showed GO sheet's strong photo response not only in ultraviolet range but also in visible range, which indicated a huge potential for light application.

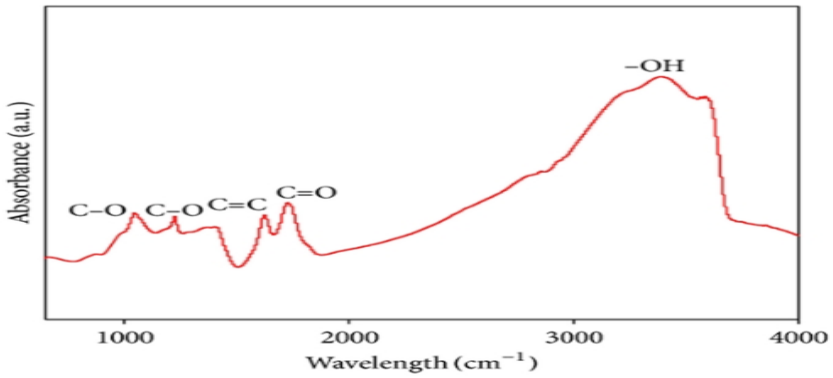

Figure 33: Absorbance peaks

4.2.5. The Thermal Stability of GO Sheet

TGA analysis were performed to check GO sheet thermal stability. Results indicated in Figure (b). The consistency loss cure of the GO sheet was observed in three phases. Next, a consistency loss of around 2 percent occurred at 100 ° C temperature, mainly due to the loss of H2O molecules in the GO sheet layers. Second, the thermal decomposition of unstable oxygen-containing functional groups showed a consistency loss of approximately 32 per cent, occurring at a temperature of 225 ° C. Eventually, an efficiency loss of 45 percent occurred at 620 ° C primarily due to carbon skeleton combustion. The findings of the study showed that GO sheet has excellent thermal stability. Graphite oxide was a normally very stable substance.

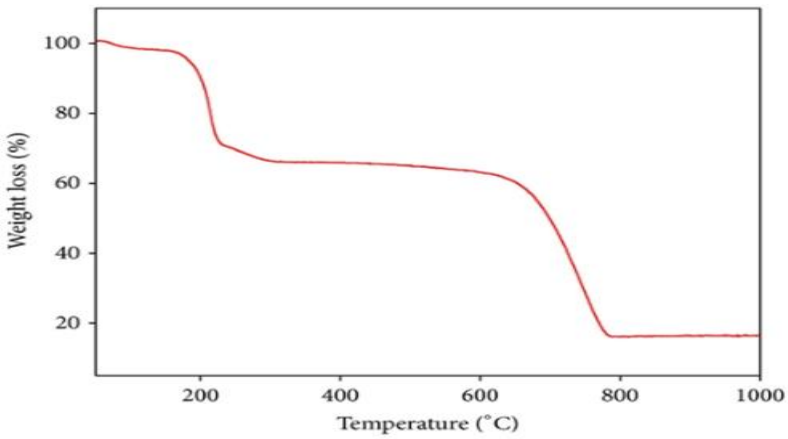

Figure 34: TGA of GO

4.2.6 The Elementals Synthesis of GO Sheet

The added mass of pure graphite was 5.0 g during the process of preparation of the GO sheet using the modified Hummer method, and the final quantity of the collected GO sheet was about 11.1 g. From this, we can theoretically conclude that the content of C variable in GO sheet was about 45.0 percent, which was consistent with the EA analysis experimental results as shown in Table. Additionally, H (3 percent) and S (0.9 percent) were found on the GO sheet, mainly due to the presence of functional groups containing oxygen incorporated in the GO sheet. Meanwhile, the quality of the O factor in the GO film was about 51 per cent based on the EA tests.

Table 3: Elemental Analysis of GO

Element%	C%	H%	S%	N%
GO	44.2	3.0	0.9	0.00

4.2.7. The XPS Analysis of GO Sheet

XPS research was performed in order to further illustrate the presence of functional groups that contain oxygen. The consequence is shown in Figure. GO XPS exhibited important signals of C and O corresponding to GO's binding capacity. Figures show the relevant C signal peak with a 285.0 eV binding energy which can be attributed to the functional groups C= C, C–C and C–H.

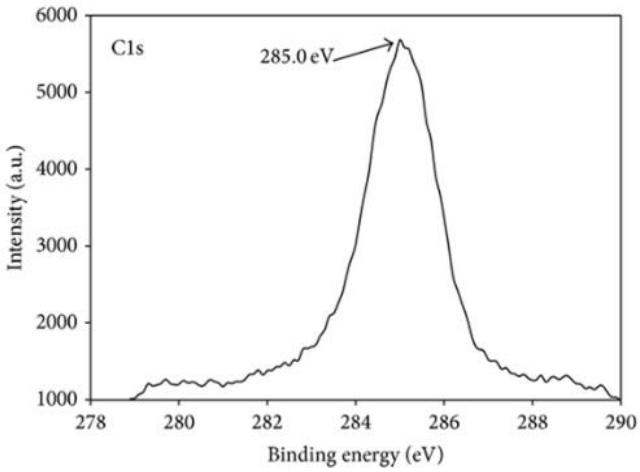

Figure 35: XPS of GO

4.2.8 Structural Analysis of Graphite Oxide (GO)

A particular branch of graphene research was graphene oxide (GO). It can be considered by either thermal or chemical reduction processes as a precursor to graphene synthesis. The graphite oxide (GO) schematic structure was shown in Figure below. GO sheets are indicated to be considered as the combined structure of functional groups containing oxygen, such as C – O, C = O, and −OH, supported on the surface of a single layer of graphene sheets. The addition of functional groups that contain oxygen modified GO sheet structure and properties.

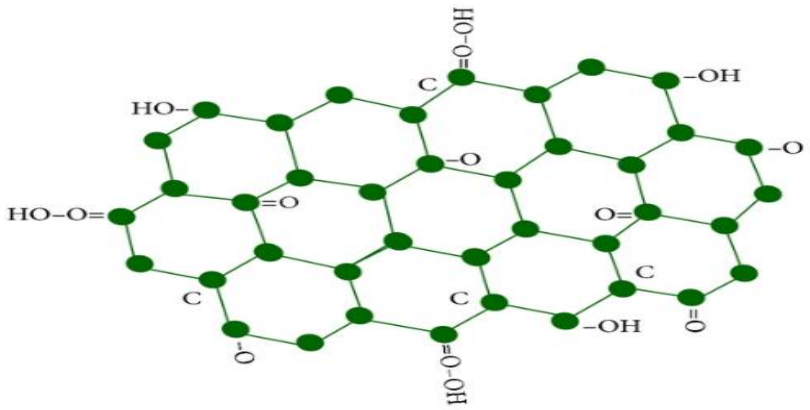

Figure 36: Structural representation of GO

Compared with single layer graphene, on the one hand, the presence of functional groups containing oxygen actually greatly improved GO sheet defectiveness. This could result in some loss of electrical conductivity, likely restricting GO's direct application in many areas.

4.2.9 Conclusion

GO films were prepared with success using adapted Hummer process. The SEM analysis showed good preparation on microscopic morphology of GO films. The GO surface with a monolayer was about 2-3 nm thick.

Further evaluating the effective preparation of GO sheets was the occurrence of oxygen-containing groups and characteristic peaks in FT-IR and XRD analysis. Lastly, EA indicated about 51 percent of the component of O elements in GO films; C, H, and S elements were also observed. The presence of functional groups that contain oxygen created more opportunities for potential GO applications in many areas. These data will provide a reference for further study of the graphene and graphene oxide character.

4.3 Results Analysis for rGO:

4.3.1 X-Ray Diffraction for rGO

As shown in Figure (a). Flake graphite shows a very sharp basal diffraction peak (002) at 2θ= 26.5 degrees (spacing= 0.33630 nm). At 2θ= 54.8 ° (spacing= 0.16738 nm), there is also a very weak diffraction peak (004). The diffraction peak (004) is the second diffraction of the diffraction peak (002) according to the rules of microcrystal layer spatial arrangement; therefore diffraction peak (004) is much weaker than diffraction peak (002). The diffraction peak at about 2θ= 9.8 ° is very typical of GO; in its XRD pattern, no apparent diffraction peak was found for rGO. This outcome is close to that of Tapas Kuila, who had defined XRD's GO and rGO structure already. In the increased GO pattern, the diffraction peak at 2θ= 9.8 ° (spacing= 0.88160) is broader and the significant increase in spacing is believed for the following reason: oxygen functional groups intercalate in the graphite interlayer. At 2θ=42.3 °, there is a very low diffraction point, which is assumed to be due to incomplete oxidation. As shown in Figure, the XRD pattern of rGO shows a very low and small diffraction peak at 2θ= 25–30 °; the diffraction peak of rGO is so weak that it cannot be seen when drawn together with graphite and GO (Figure a) in the XRD pattern. At 2θ=42.3 °, there is also a low diffraction point.

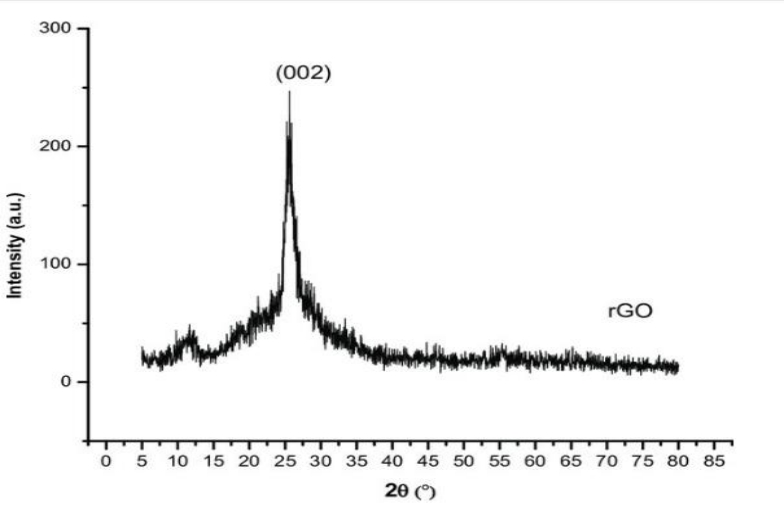

Figure 37: XRD of rGO

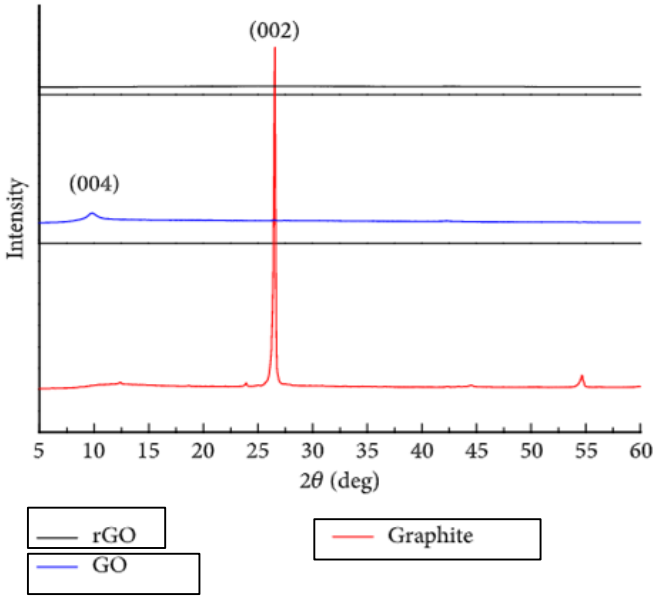

Figure 38: xrd comparison

4.3.3 FTIR for rGO

FTIR spectra of GO and rGO are shown in Figure, where it indicates certain functional carbon-oxygen groups of GO, such as O–H, C= O, C–OH, and C–O. It is estimated that the characteristic peak (~3464 cm−1) is attributed to O–H stretching of hydroxyl and carboxyl groups, and characteristic peaks of C= O (~1639 cm−1), C–OH (~1288 cm−1), and C–O (~1003 cm−1) are also attributed to carboxylic acid and carbonyl groups. And the characteristic value at 1493 cm−1 corresponds to the un-oxidized graphic domain C = C skeletal vibration. Such functional oxygen groups suggest the oxidation of the flake graphite powder to GO. As shown in Figure, no apparent peak could be observed, meaningful GO reduction had been made.

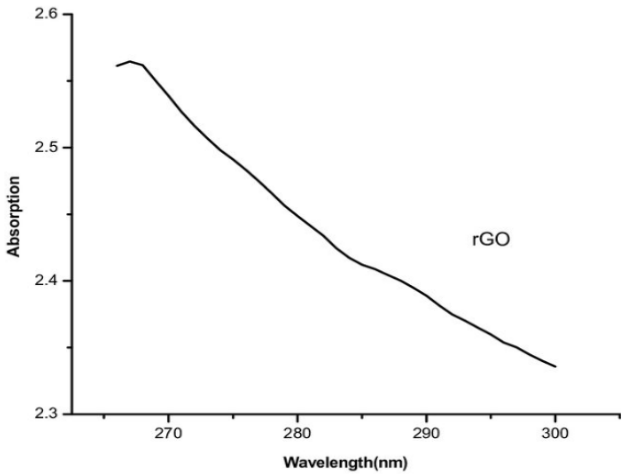

Figure 39: FTIR of rGO

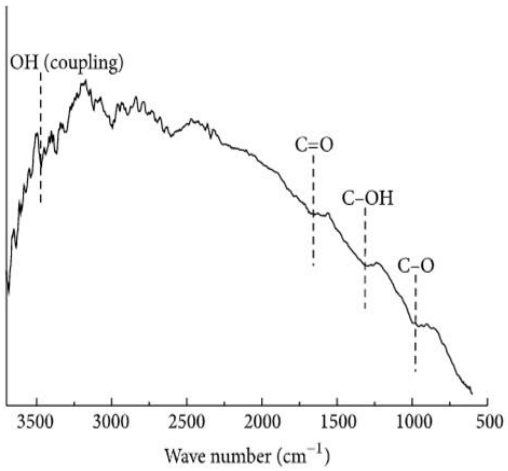

Figure 40: functional groups in rGO

4.3.3 SEM for rGO

Figure a shows rGO SEM morphologies which were dried for 1 day at 80 ° C. It is possible to observe 2-dimensional material, as shown in Figure. Fold structure can be found at both the rGO powder surface and bottom. We are typical of few-layer rGO morphologies. The thickness of rGO may be 10 nm, and it is clear that rGO layers have relatively large dimensions (much larger than 100 nm) and that rGO is restacked. The explanation for the re-agglomerate may be the long-term treatment of high temperatures. The graphite morphology (fold structure) can also be found in Figure.

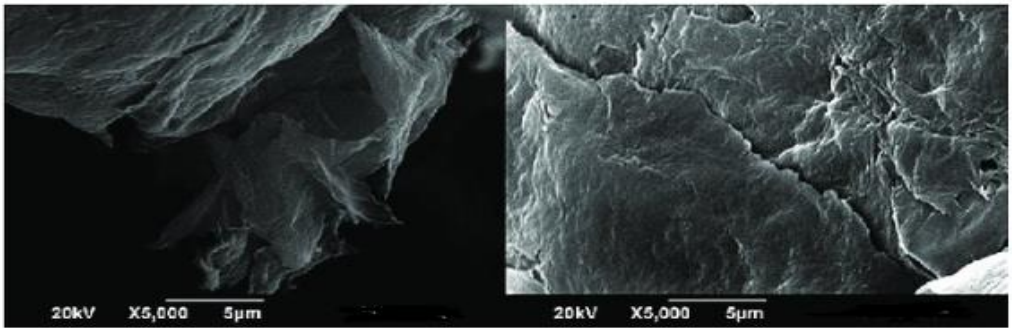

Figure 41: SEM of rGO

4.4 Results for AgNP (spherical)

4.4.1 SEM for AgNP:

Nanoparticles attached to aluminum stubs in sample preparation use double-sided carbon tape for sample mounting remove loose sample material by gently pushing the holder onto a hard surface. For topographical imaging move the stub with sample directly to the SEM. The characterization in FEI SEM Quanta 200 was carried out.

SEM images are shown in 10,000X and 20,000X magnification figures. The results of secondary electrons indicate that particles in shape, dispersive & crystalline in structure are almost identical spherical. It is possible to measure the diameters of the polycrystalline particles using the scale shown in each micrograph and the measured range is written with each figure below.

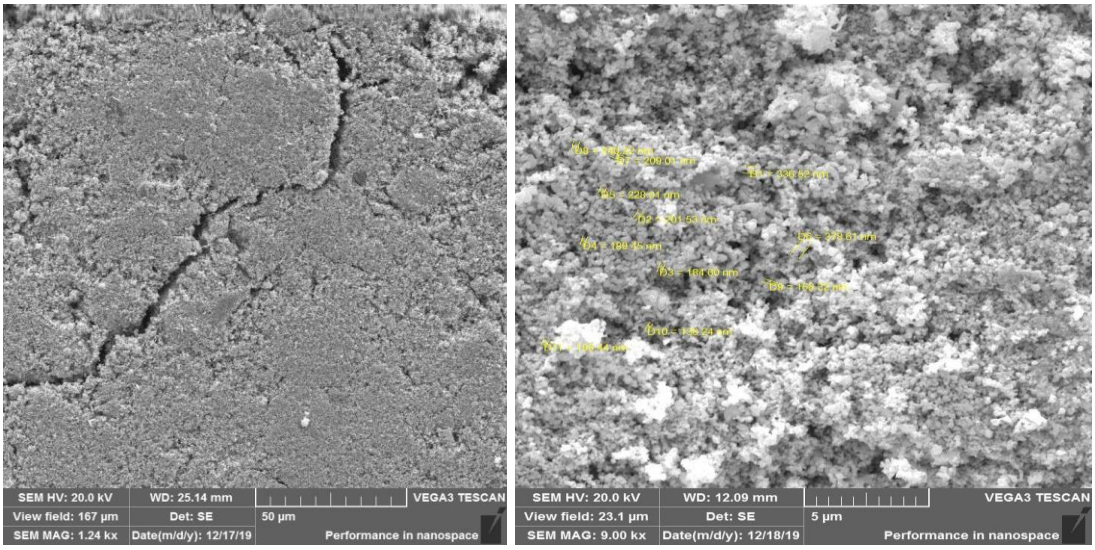

Figure 42: SEM of AgNP

4.4.2 EDX for AgNP

Elemental compositional analysis was also carried out by means of EDS (Energy Dispersive Spectroscopy) to determine the purity of silver nanoparticles. Since there is a huge difference in the atomic number of oxygen & silver, the comparison of the atomic number of these two elements is mainly a method for weight percentage detection. Results are summarized in Table; shows 98.06 percent by weight & 88.11 percent by silver atom nanoparticles & only 1.96 percent & 11.89 percent by oxygen were present respectively. Graphically the results are shown in Graph which is an automated generated graph by built-in SEM software showing the highest silver counts. The presence of oxygen indicates that by forming silver oxide, certain particles have been oxidized & agglomerated, but it is a very minute amount, the others are still stabilized.

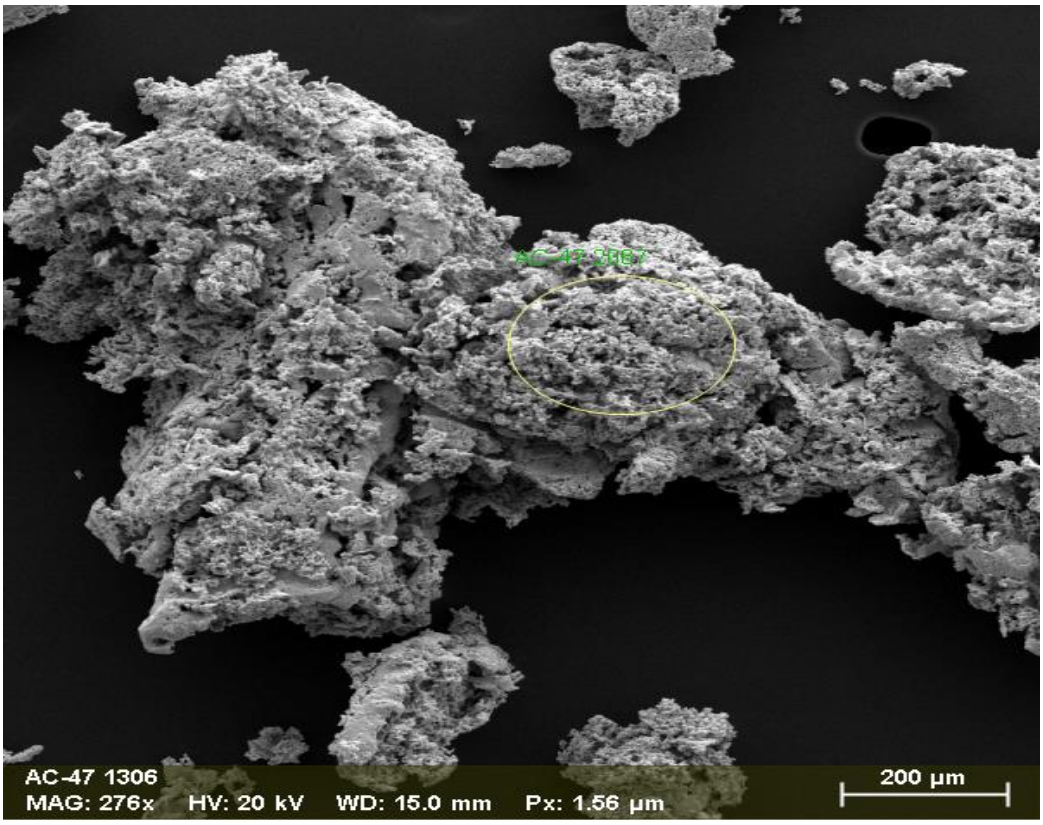

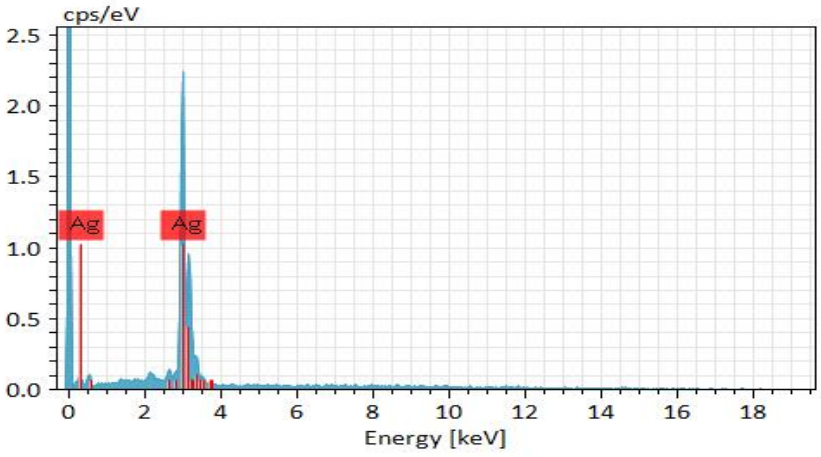

AC-47 2067

Element	At. No.	Netto	Mass [%]	Mass Norm. [%]	Atom [%]	abs. error [%] (1 sigma)	rel. error [%] (1 sigma)
Silver	47	7732	100.00	100.00	100.00	2.74	2.74
		Sum	**100.00**	**100.00**	**100.00**		

Figure 43: EDS analysis of AgNP

4.4.3. Particle Analyzer for AgNP:

The distribution of particle size is best measured quantitatively by analysis of the Laser Particle Analyzer. First run the standard solutions of known size distribution to find the distribution, the detectors record the energy dispersed & absorbed at a particular angle & make dispersing patterns then compare sample values with those standard values. BT-9300H Better Size Instrument had been used for particle size analysis.

The mean particle distribution of silver particles was found by eight different samples. The recorded distribution of each individual sample is shown in the histogram.

Histogram results show 100%, 50% in 300-310 nm, 5% in 310-320 nm, 30% in 320-330 nm, 40% in 330-340 nm and 5% in 340-350 nm silver particles, the same sequence of analysis will also be observed for particle distribution in sample 2,3,4,5,6,7 and 8.

Table 4: Graph of EDX

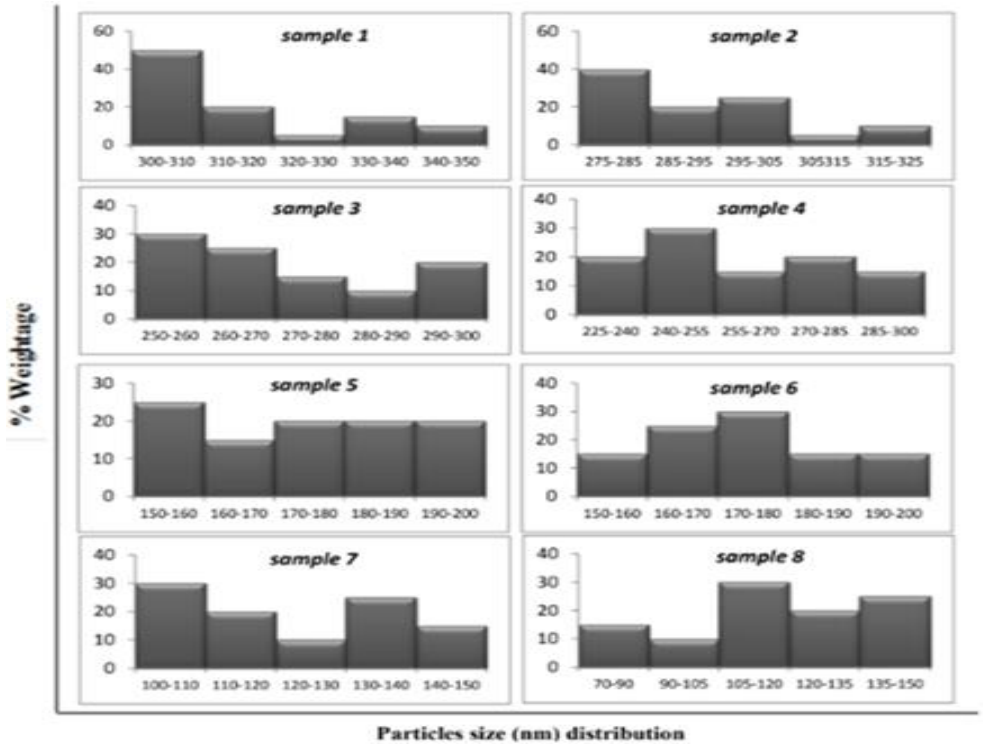

4.4.4. FTIR for AgNP:

Fourier Transforms Infrared Radiation (FTIR) serves as the molecular fingerprint for the identification of organic materials. This technique is extremely useful for the confirmation of the presence of carboxylic acid on the silver nanoparticles as a coating. The FTIR spectrum collected of the organic material found in the sample compared with spectra libraries cataloged for known materials for the best matches. There are five large peaks that can be seen at 3469, 2370, 1653, 1571, 1506 cm-1 in figure 5 of silver particle spectra.

The first peak at 3469 & 1571 cm-1 assigned to hydroxyl group, because in the oxidation of the hydroxyl group remains unreactive & also some moisture get absorb on the highly reactive surface of nanoparticles. The peak at 2370cm-1 belongs to (CH) stretching band of aldehyde group, some solution not succeeded to oxidize to carboxylic acid & the peak at 1550 & 1506cm-1 was concluded to be Nitrate from AgNO3, which is starting metal precursor, when we compared the standard FTIR spectra of silver nitrate.

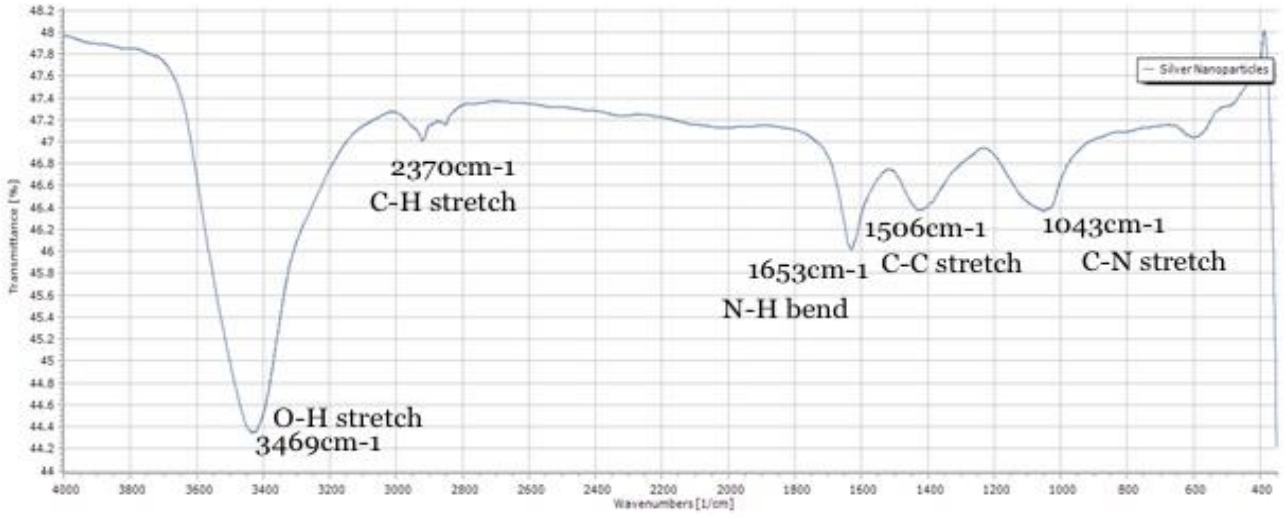

Figure 44: FTIR of AgNP

The absorption of C=0 is one of the spectrum's most characteristic. Ketone is called the root compound whereas the derived structures are the aldehyde & carboxylic. At1653 cm-1 the characteristic peak of carboxylic acids is shown in the figure's expanded spectra. The frequency range of carboxylic acids is 1700–1300 cm-1. As far as the hydroxyl group has

direct interaction with the carbonyl group, they are unique in signature by forming a stable hydrogen-bonded structure.

In the enlarged spectra Figure, when this segment will match all major & minor peaks compared to standard spectra, the carbonyl peaks are present at 1571cm-1 with the hydroxyl group, which confirms the presence of carboxylic acid on the surface of silver particles.

4.4.5 XRD for AgNP:

X-Ray Diffraction (XRD) research looked at the structure of prepared silver nanoparticles. The silver nanoparticles dry powder is used for XRD analysis. The diffracted intensities were measured at 2θ from 20 ° to 80 °. The sample XRD pattern, prepared by the chemical method presented here, is shown in the Figure.

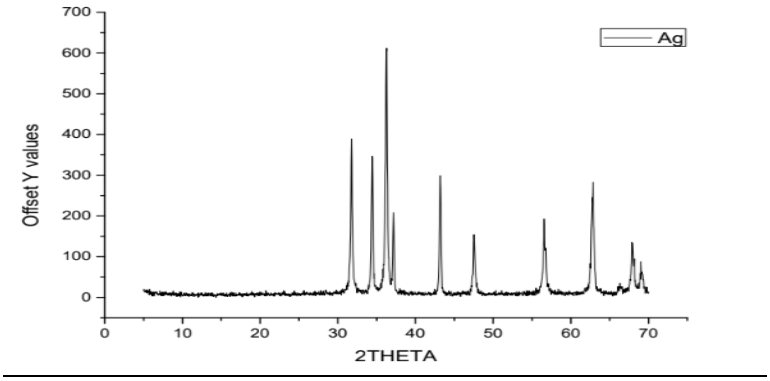

Figure 45: XRD of AgNP

The nanoparticles of powdered silver show a cubic structure showing peaks at 2 theta= 38.331 (111), 44.488 (200), and 64.644 (220). For FFC material the high intensive peak is (111), which is observed in the powdered sample.

Table 5: xrd spectrum

Observed 2Θ values	d values Angstrom	Intensity Count	Intensity Percentage
38.331	2.34634	1239	100
44.488	2.03484	500	40.3
64.644	1.44068	372	30

Table 6: Evaluation of XRD spectrum

Peak No.	2Θ	(SinΘ)^2	1*(SinΘ)^2/(SinΘ min)^2	2*(SinΘ)^2/(SinΘ min)^2	3*(SinΘ)^2/(SinΘ min)^2	h^2+k^2+l^2	hkl
1	38.331	0.107	2.00	2.00	3.00	3	111
2	44.488	0.143	2.67	2.67	4.00	4	200
3	64.644	0.285	5.32	5.32	8.00	8	220

4.4.6 Conclusion on Characterization:

Synthesized by wet chemical pathway, the Silver nanoparticles are characterized by the use of SEM, LASER Particle Analyzer, FTIR spectrometry and XRD techniques. The mean particle size is in the range of 120-325 nm. DEA concentration plays a crucial role in controlling particle size. This research also demonstrates a rapid route to efficiently synthesize large-scale quantities of Silver nanoparticles using industrial grade chemicals while preserving the purity and properties. For its heat transfer properties and use in Nano fluids and conductive gels, these Silver Nanoparticles can be further studied in the future.

CHAPTER 5

SENSOR RESPONSE

5.1. Proposed silver Nano-particles doping

The high specific surface area of the GO sheets makes them an appropriate platform for entrapping silver nanoparticles. Once the silver nanoparticles are entrapped between the reduced GO sheets, the possibility of their agglomeration significantly declines while their release and free movements are extremely restricted. It is then expected that the combination of silver nanoparticles with reduced GO sheets have more desirable sensing function compared to graphene oxide alone.

5.2 Formation of AgNP/rGO film

In our route the reduced GO was used as starting material, and the obtained Nano-composites were designated rGO/AgNP. For the preparation of these samples, 25 mg of GO was dissolved in 50 mL DH_2O, and ultra-sonicated for 45 minutes using a water bath sonicator. It was then mixed with 50 mL $AgNO_3$ (final concentration = 6 mM) and a gray transparent film formed spontaneously at the interface.

The coupled Nano system of rGO-Ag was synthesized by mixing GO and Ag in a 2:1 ratio in 50 mL of distilled water.

5.3 Screen Printing

Screen printing is a printing technique where a mesh is used to transfer ink onto a substrate, except in areas made impermeable to the ink by a blocking stencil. The steps can be explained by following figure:

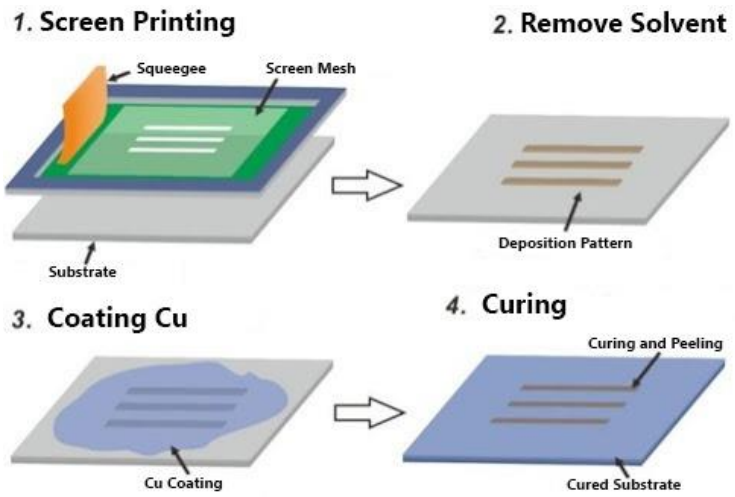

Figure 46: Screen Printing Steps

The screen printing of our substrate can be seen in the figure below:

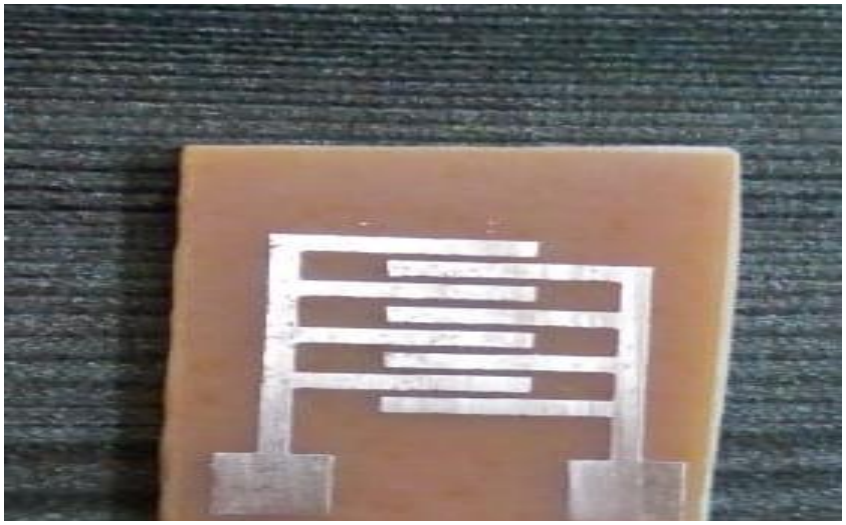

Figure 47: screen printing on our substrate

5.4. Deposition of AgNP/rGO:

For small substrates (~1 cm^2), an easy and tunable deposition method is drop-casting where spreading a nanoparticle dispersion over a substrate and allowing it to dry under controlled conditions, i.e. pressure and temperature. In principle, film thickness depends on the volume of dispersion used and the particle concentration, both of which can be easily varied. There are also other variables that affect the film structure such as how well the solvent wets the

substrate, evaporation rate, capillary forces associated with drying, etc.

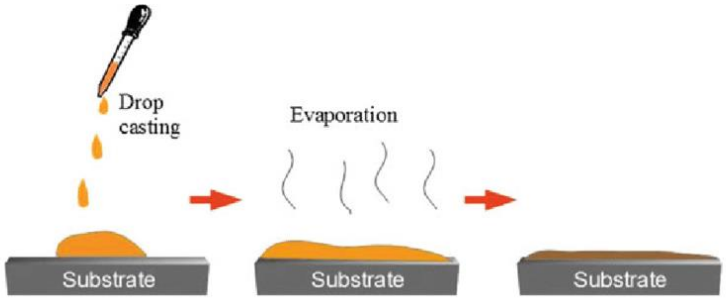

Figure 48: Drop Casting Steps

Deposition of Nano composite films on substrates was performed as follows: clean substrates were put in a beaker, and the final system (film) was entirely transferred to the beaker. With the aid of tweezers/pipettes, the substrate was pulled out of the beaker, and a film was deposited on the substrate.

The thickness, roughness and transmittance of these films are presented in following table. As can be seen, an increase in the concentration of $AgNO_3$ during the samples preparation increases both the thickness and roughness (more than 100%) of the films, and decreases their transparence. These effects are directly related to the increase in the amount of the silver nanoparticles and the agglomeration of these particles.

Table 7: Thickness and transmittance of film

Film	Thickness(nm)	Transmittance (%)
rGO	~109	86
rGO/AgNP-1/0.5	~175	78
rGO/AgNP-1/2	~195	68
rGO/AgNP-1/5	~280	55

In summary, our route present novel and simple route to synthesize graphene/silver nanoparticles materials, obtained directly as thin, transparent and transferable films, based on a liquid–liquid interface. The route is innovative because the material is prepared and

processed (as thin film) directly in one-pot reaction, without the utilization of chemical stabilizer for the silver nanoparticles.

The important variables as film thickness and transmittance can be easily controlled simple by varying the diameter of the liquid–liquid interface.

5.5. The Response Measuring Setup

Having described the manner of decorating graphene sheets with silver nanoparticles, we devote the present section to the experimental setup we use for characterization of graphene decorated with silver nanoparticles (AgNPs/rGO) as a methane gas sensor. To this end, an ideal schematic representation of the setup is illustrated where Sensor response to methane gas was measured using a home-built system consisting of a closed chamber with sensor holder, gas source and Agilent Multi-meter. The test gas was generated according to desired concentration and allowed to enter in testing chamber. The setup is shown in figure below:

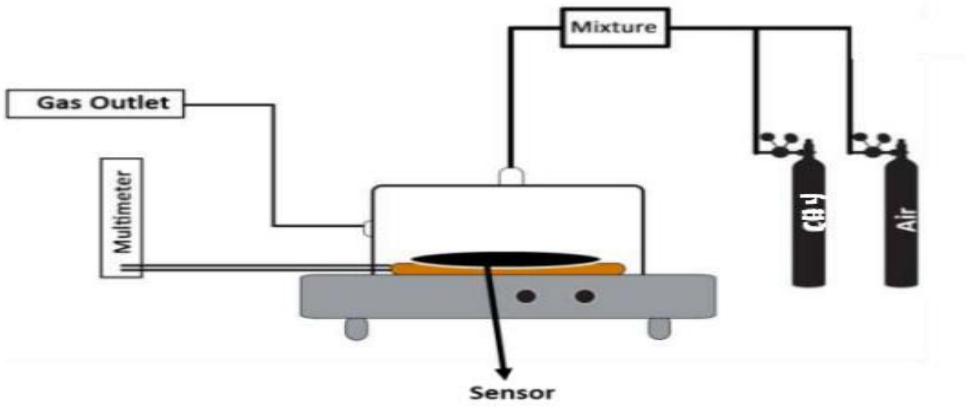

Figure 49: response measuring setup

5.5.1 Sensing element

PVC board coated with copper was brought from the local market and cut into an appropriate size. The construction of circuit based upon it by screen printing. The resulting chip was dipped into aqueous hot solution of FeCl3 in the next step, which resulted in extra copper

and copper-integrated electrode (IE) being extracted. The resulting products (bare rGO, rGO/AgNP film) were deposited using drop casting on IE.

The gas sensor in following figure consists of inter-digitated Ag–Cu electrodes of 150 μm width, spaced equally at the same pace, onto which grains of graphene plaster of the previous subsection have been dropped. The separate digits are printed on a masked substrate of printed circuit board (PCB). The decorated graphene sheets then stipulate a connection between the digits.

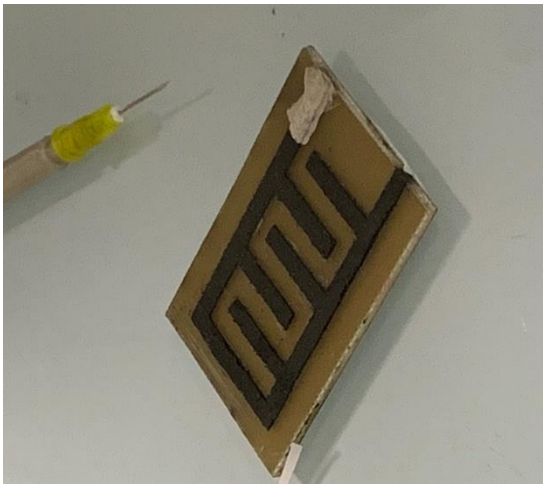

Figure 50: formation of Ag electrodes

Moreover, to provide thin and almost uniform distributions of graphene sheets over the electrodes, the plaster was first diluted and ultra-sonicated. In our experiments, drops of volume 10 μL would be most efficient. The combination was then placed in an oven of temperature 45°C so that a solid thin pill of decorated graphene resided onto the electrodes.

5.5.2 Prototype of Sensor:

The entire system (Arduino module, external ADCs and PC) and the signal processing were controlled by an in-house developed software in Labview Environment (National Instruments).

The figure below of our prototype shows the possibility of implementing such a detector using a programmable board and the Arduino Nano memory. There are a couple of dozen contacts on the board, to which you can connect not only a number of chemical gas sensors

developed by us but also all kinds of components: displays, LEDs, other sensors, motors, routers, magnetic locks, etc. It is possible to load a program into the Arduino processor that will control all of these devices according to a given algorithm. The Arduino board provides extensibility and the ability to automate certain activities.

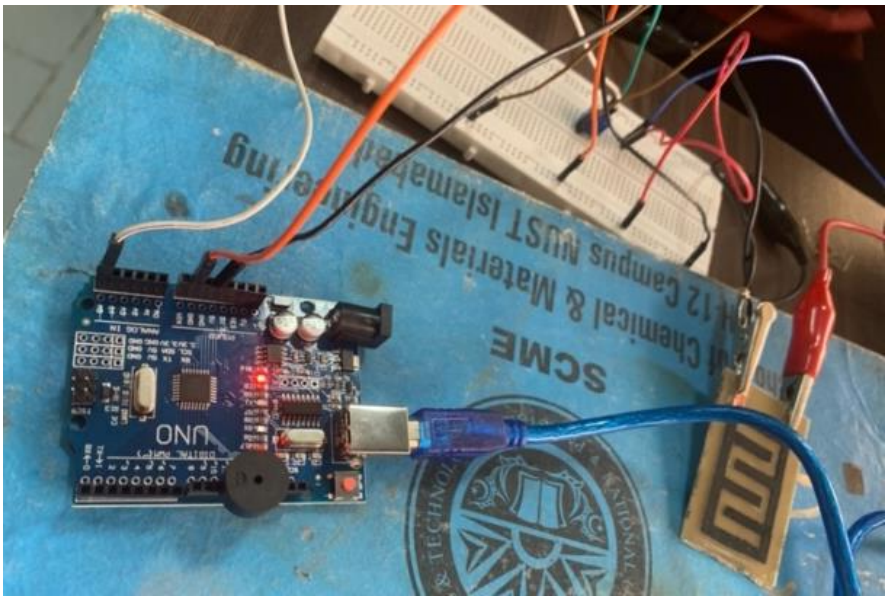

Figure 51: Our prototype consisting of Arduino, board, substrate etc.

In addition to the Arduino board, and the gas sensor, we needed an alarm system and buttons to turn the system on and off. The entire system is powered by six finger batteries or an AC-DS adapter. This device allows us to measure methane gas even at very low concentration.

5.6 Sensor Response

To measure the sensing performance, the gas sensor is first allowed to attain its stable resistance at room temperature (baseline resistance) and then the methane gas was injected into the sealed chamber, in which the sensor was placed. The gas sensor is kept at a constant temperature, T. The CH4 concentration was controlled by adjusting regulator knob of CH4 gas cylinder to air inside the chamber.

After the senor resistance attains a steady state on its saturation, CH4 gas was exhausted from the chamber through air flow into it. The electrical resistance was recorded by the

multimeter until the sensor resistance almost attained its baseline value (the same value as in the absence of gas).

The change in resistance with time was measured by multi-meter. The percentage response was calculated from given formula;

$$\%R = \frac{R_{gas} - R_{air}}{R_{air}} \times 100$$

According to this definition along with the sensing mechanism of our proposed material presented, a positive value of response, %R indicates an increase in sensor resistance due to the electron donation of gas molecules, while a negative value corresponds to a reduction of sensor resistance arising from the electron-accepting behavior of the gas molecules.

In addition to response, another parameter of interest in the design of sensors is the so-called response and recovery time scales. We define the response time as the duration for which, in the presence of gas, the response reaches 90% of its maximal (stable) value.

Where recovery period is time it takes, in the absence of gas, for the response to reach 10% of its stable value.

IV characteristics for methane sensing clearly show the shift of the peak with the exposure of the gas for our sensing element. Sensor when exposed to maximum flow of methane gas i.e 150 sccm, it shows change in resistance very rapidly.

Table 8: sensitivity of methane gas sensor

Conc. of Methane (sccm)	**Sensitivity (Ra/Rg)**
150 sccm	1.04

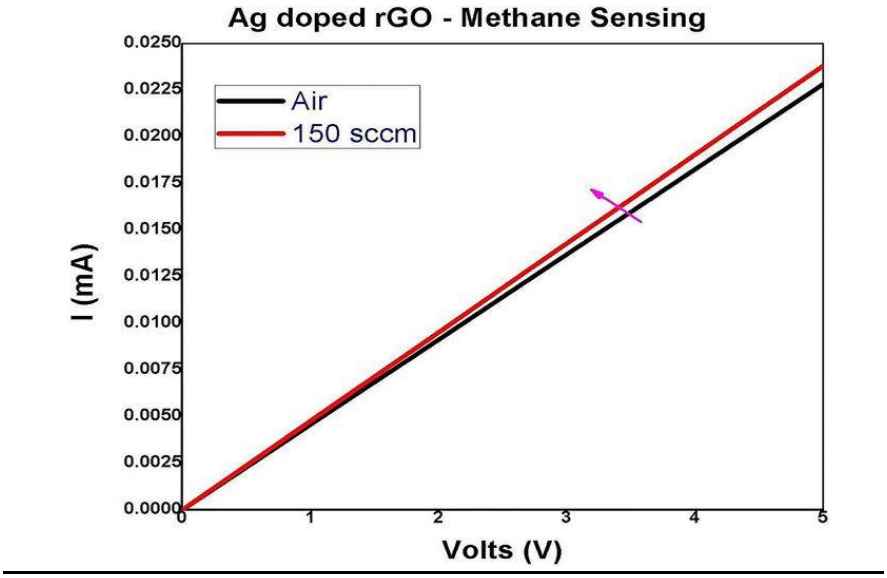

Figure 52: IV graph of methane gas sensor

Silver Nano-particles doped rGO sensor shows p-type behavior. The graph below shows the response of AgNP-doped rGO sensor towards 150 sccm of CH4. Dynamic response curve have three regions;

- Response region.
- Saturation region
- Recovery region.

As graph show sensor response rise with the exposure of CH4 gas and reach to Saturation plateau after saturation curves move to desorption mode which represent the recovery of sensor.

Table 9: response, recovery time of sensor

Response time	30 sec
Saturation duration	130 sec
Recovery time	140-180 sec

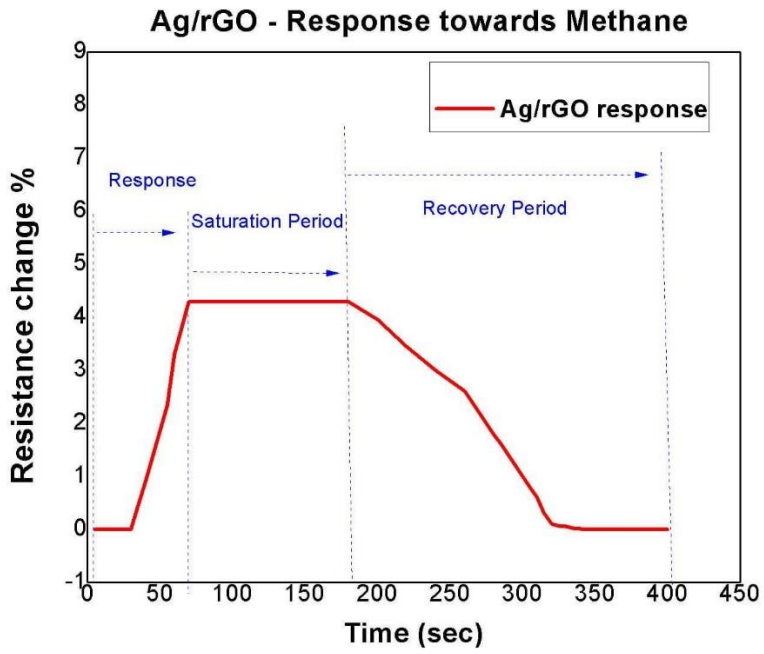

Figure 53: response graph of gas sensor

A comparative study shows how bare rGO responds to methane in comparison to AgNP doped rGO. All the three factors; response time, recovery time and sensitivity are better when reduced graphene oxide is doped with silver Nano particles.

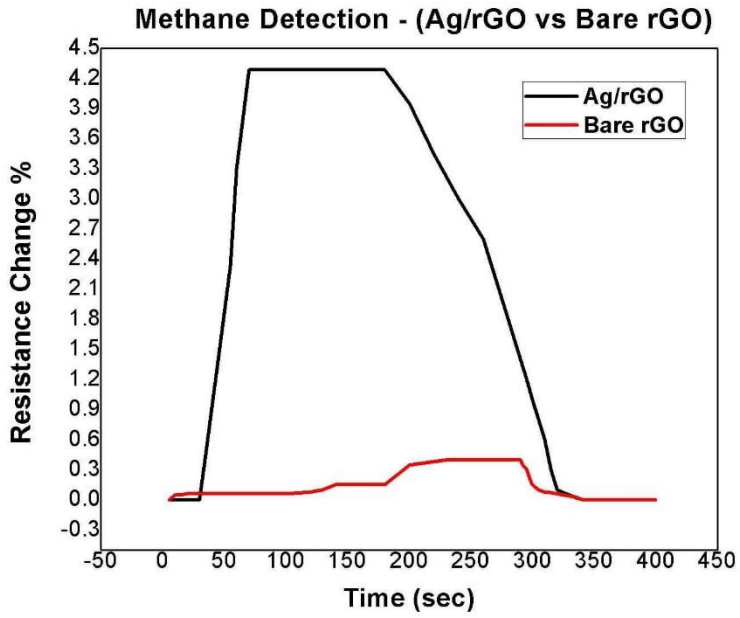

Figure 54: Comparison between bare rGO and doped rGO

It is clear from this figure that as graphene is decorated with more silver nanoparticles (larger mass ratios), the response of the device increases drastically. Meanwhile, the response time becomes much shorter since the number of active sites (AgNPs) increases, adsorption of CH4 onto the sensing material occurs more frequently; thus, the number of electrons delivered to graphene, in a fixed period, also increases, leading to shorter response time. Another point of interest, concluded from this figure, is the fact that after the recovery time, the residual gas on the device is almost completely absent.

5.7 Comparative study

Finally, to make a comparison between the performance of our device and some of other compatible recent proposals, we present the following table.

Table 10: Literature work on methane gas sensor

GAS	HYBRID MATERIAL	TEMP C	DETECTION RANGE (delta L/L)	CONC. (delta L/L)	RESPONSE TYPE	SENSOR RESPOSE	τ(res)/τ(rec) (s/s)	reference
CH4	PANI/rGO	RT	10-3200	100	Rair/Rgas	~3	85/45	Wu et al.,2013
	NiO/rGO	260	100-6000	100	ΔR/Rair	~2.2%	6/16	Zhang et al., 2016
	ZnO/rGO	190	100-4000	1000	ΔR/Rair	~12%	~200	Zhang et al., 2015b
	SnO2/rGO	150	1000-10000	1000	ΔR/Rair	47.6%	61/330	Navazani et al., 2018
	Pd/SnO2/rGO	RT	800-16000	14000	ΔR/Rair	9.8%	5/7 min	Nasresfashani et al, 2017

From the information contained in the table, one arrives at the conclusion that there is no ideal material for forming a gas sensing device: every proposal so far is in some regards advantageous, while disadvantageous in other respects. For instance, some methane gas sensing materials detect lower gas concentrations very fast with a high response, but operate at very high temperatures or exhibit low reproducibility, selectivity, and stability. Table clearly specifies the advantages of our device over the compatible ones. It is worth noting from table that the proposed sensing material operates well at room temperature with much wider detection. Moreover, as previously mentioned, the sensor is fabricated by dropping the grains of graphene plaster on the Ag−Cu interdigitated electrodes printed on a substrate of PCB which is of very low cost. This type of substrate has a great electrical isolation to avoid current leakage, improving sensor reliability. It also aims sensor integration with related electronics circuits, either driving or readout, which are usually implemented on such substrates.

5.8 Conclusion

The present report is concerned with the design of a methane gas sensor using graphene decorated with Ag nanoparticles. To analyze the formation of Ag nanoparticles and the result of decoration, we present Figures, where an SEM images of plain graphene and silver nanoparticles are exhibited. The first part indeed demonstrates that, in our sample, graphene sheets are of high quality, while the rest of the figure indicates the formation of Ag nanoparticles with a size of 120-320 nm. The advantage of our method (Section 3), in addition to being more environment friendly, is that the final product is free of extraneous elements. To support this claim, we also present the results of an EDS test. We then proceed by placing the final product onto inter-digitized electrodes and measure the resistance of the device. The response of the device, as defined in terms of the change in resistance. The following more interesting characteristics of the device, as a methane gas sensor, are drawn:

• The device exhibits a fairly high response toward methane gas even at relatively low temperature i.e. room temperature.

• After the elapse of the recovery time, the response of the device returns almost completely to its original value. Consequently, the device is reversible.

• The sensing device is also highly repeatable as well as stable.

• The proposed sensing material reacts to the presence of methane gas in a natural way so that no external stimulus/heating element is needed to initiate its performance.

• The signal-to-noise ratio of the device, because of Ag decoration, is quite large in comparison to plain graphene.

• The response of the device is selective and reacts very weakly toward other dominant gases in the environment. Our proposed device, therefore, is capable of performing under ambient conditions.

According to the above points, the present article indeed proposes a novel device for methane gas sensing, with favorable characteristics at low temperatures.

5.9 Future directions

The project can be taken into the following directions in terms of research as well as commercialization:

- **Research Directions:**

- The behavior of response versus time for different temperatures with a fixed mass ratio of AgNP: rGO can be studied.
- The device response, as a function of time, for different mass ratio, at room temperature (25 °C) can be improved.
- To examine the repeatability and long-term stability, consecutive response measurements, as a function of time can be studied.
- The effect of humidity on the device performance.

- **Commercialization Directions:**

- Collaborating with CAC, Research, Innovation, and Commercialization (RIC) sectt, NUST to develop the required circuit, proposed in FICS 2020, for developing a functional real-time sensor.
- Tuning the current configuration to achieve detection of gases required in oil and gas industries to establish a local market and strategic institutions like NESCOM (current sensors are being imported).
- As the chemical sensors market is expected to expand at a compound annual growth rate of 8.1%, and in 2024, reaching USD 40.8 billion globally. The integration of chemical sensors in electronics will be the major driving force of this market growth so it has a potential for startup.

REFERENCES

1. https://www.researchgate.net/publication/275330559_Graphene_film_doped_with_silver_nanoparticles_Self-assembly_formation_structural_characterizations_antibacterial_ability_and_biocompatibility
2. https://pubs.acs.org/action/showCitFormats?doi=10.1021/acsami.9b00625
3. https://www.hindawi.com/journals/jnm/2015/168125/
4. https://doi.org/10.1155/2014/276143
5. Muhammad Muzamil et al 2014 IOP Conf. Ser.: Mater. Sci. Eng. 60 012034
6. J. Davies, "Hazardous Gas Model Evaluation with Field Observations." Atmospheric Environment, vol. 29, no. 3, 1995, pp. 456–457.
7. J. Chou, Hazardous Gas Monitors: a Practical Guide to Selection, Operation and Applications. McGraw-Hill, 2001.
8. G. Korotcenkov, "Metal Oxides for Solid-State Gas Sensors: What Determines Our Choice?" Materials Science and Engineering: B, vol. 139, no. 1, 2007, pp. 1–23.
9. I. Eisele, T. Doll, M. Burgmair, "Low Power Gas Detection with FET Sensors." Sensors and Actuators B: Chemical, vol. 78, no. 1-3, 2001, pp. 19–25.
10. Noboru. Yamazoe, "Toward Innovations of Gas Sensor Technology." Sensors and Actuators B: Chemical, vol. 108, no. 1-2, 2005, pp. 2–14.
11. G.Ruess and F.Vogt. High-lamellar graphite oxide. "Monatsh. Chem." vol.78, no. 3, 1948, pp.222–242.
12. Studies of Reduced Graphene Oxide and Graphite Oxide in the Aspect of Their Possible Application in Gas Sensors Sabina Drewniak 1,, Roksana Muzyka, Agnieszka Stolarczyk Tadeusz Pustelny Michalina Kotyczka-Mora, ´nska and Maciej Setkiewicz Vijay K Varadan, A Sivathanu Pillai, Debashish Mukherji Nanoscience and Nanotechnology in Engineering 2009 (Scientific Publishing Co. Pte Ltd., Singapore).
13. https://www.frontiersin.org/articles/10.3389/fchem.2018.00399/full#B21
14. S. Park and R. S. Ruoff, "Chemical methods for the production of graphenes," *Nature Nanotechnology*, vol. 5, no. 4, pp. 217–224, 2009.
15. S. Stankovich, D. A. Dikin, R. D. Piner et al., "Synthesis of graphene-based nanosheets via chemical reduction of exfoliated graphite oxide," *Carbon*, vol. 45, no. 7, pp. 1558–1565, 2007.
16. A. Bagri, C. Mattevi, M. Acik, Y. J. Chabal, M. Chhowalla, and V. B. Shenoy, "Structural evolution during the reduction of chemically derived graphene oxide," *Nature Chemistry*, vol. 2, no. 7, pp. 581–587, 2010.
17. H. Zhang and P. X. Feng, "Fabrication and characterization of few-layer graphene," *Carbon*, vol. 48, no. 2, pp. 359–364, 2010.